Magneto-photo-thermoelastic Interactions in a Semiconductor Solid Cylinder Due to a Periodic Decaying Varying Heat

A. E. Abouelregal
Mansoura University
Ashraf M. Zenkour (zenkour@gmail.com)
King Abdulaziz University https://orcid.org/0000-0002-0883-8073

Research Article

Keywords: Photo-thermoelasticity, relaxation time, periodic decaying heat, solid cylinder, semiconductor, magnetic field

Posted Date: February 15th, 2021

DOI: https://doi.org/10.21203/rs.3.rs-226412/v1

Magneto-photo-thermoelastic interactions in a semiconductor solid cylinder due to a periodic decaying varying heat

A. E. Abouelregal[1,3] and A. M. Zenkour[2,4,*]

"[1]Department of Mathematics, Faculty of Science, Mansoura University, Mansoura 35516, Egypt
[2]Department of Mathematics, Faculty of Science, King Abdulaziz University, P.O. Box 80203, Jeddah 21589, Saudi Arabia
[3]Department of Mathematics, College of Science and Arts, Jouf University, Al-Qurayyat, Saudi Arabia
[4]Department of Mathematics, Faculty of Science, Kafrelsheikh University, Kafrelsheikh 33516, Egypt"

Abstract

In this article, a generalized photo-thermoelastic model with relaxation time (GPTE) was introduced and applied to an infinite semiconductor body in the form of a solid cylinder. The cylinder and its adjoining vacuum are constrained exposed to periodic decaying varying heat and subjected to a uniform axial magnetic field. Analytical formulas of the physical quantities of the problem were obtained using Laplace transformations. A numerical method is used to find the inverse Laplace transforms. The effect of phase-lags, the temperature frequency on the derived expressions have been illustrated graphically and discussed.

Keywords: Photo-thermoelasticity; relaxation time; periodic decaying heat; solid cylinder; semiconductor; magnetic field.

Nomenclature

λ, μ	Lamé's constants	E_g	semiconductor gap energy
α_t	thermal expansion coefficient	κ	thermal activation coupling parameter
$\gamma = (3\lambda + 2\mu)\alpha_t$	coupling parameter	n	carrier density
T_0	environmental temperature	δ_{ij}	Kronecker's delta function
$\theta = T - T_0$	temperature increment	u_i	displacement components
T	absolute temperature	F_i	body force components
C_e	specific heat	$\vec{H}$	magnetic field
μ_0	magnetic permeability	$\vec{J}$	current density
$\vec{h}$	nduced magnetic field	$\vec{E}$	induced electric field
e	cubical dilatation	τ_0	relaxation time
σ_{ij}	stress tensor	τ_1	lifetime of photogenerated electron
e_{ij}	strain tensor	ρ	material density
$d_n = (3\lambda + 2\mu)\delta_n$		δ_n	coefficient of electronic deformation
τ_{ij}	Maxwell's stress	K	thermal conductivity

***Corresponding author:**

E-mails: zenkour@kau.edu.sa, zenkour@sci.kfs.edu.sa (A.M. Zenkour)

1. Introduction

Studying the interaction between stress and the magnetic field in a thermal body is very important because of its various applications in plasma physics, geophysics, and associated subjects. Particularly in nuclear fields, the gradients of very high temperature, as well as the magnetic fields created within nuclear reactors, influence the design and physical processes. Furthermore, the earth is due to the magnetic field in general, and its materials may be electrically conducting.

To remove the contradictions inherent in the coupled and uncoupled thermoelastic models that propagate the heat at infinite speed because of the parabolic heat equation, a generalized theory of thermoelasticity is introduced by Lord and Shulman [1] and Green and Lindsay [2]. Tzou [3] announced a new model of thermoelasticity where the Fourier law is exchanged by the approximation of a heat conduction equation that includes two different phase-lags (DPLs).

As technologies developed, semiconductor materials are widely used in advanced modern engineering. The study of wave propagation in bodies of semiconductors has academic significance and practical value. The wave propagation problem in a semiconductor solid is not recorded during the photothermal process yet. In addition, the progress of semiconductor processes and fabrication over the last decades have made great efforts. The photoacoustic effect theory was developed in semiconductors for the bass region, taking into account the acoustic and phonon drag by the electron-hole couple diffusion flux [4-13]. A classic theoretical model for photoacoustic influence (PA) has been studied in the semiconductor system, which includes space charge on the semiconductor surface, thermoelastic, thermo-diffusion, and electronic deformation effects [14, 15]. Recently, Zenkour [16-18] presented a refined multi-phase-lags model for the thermomechanical response of microbeams or to treat photothermal waves of semiconductor half-space media.

The dynamic behavior of interactions between the magnetic field and temperature and pressure of the thermal solids is of great importance due to its wide uses in such diverse fields as geophysics, plasma physics, nuclear engineering, and related subjects. Using generalized thermal models, many researchers have made efforts to study thermomagnetic problems. Allam et al. [19] studied the magneto-thermoelasticity concerned with infinite solid with a spherical cavity when the properties of the material are variables. Abouelregal and Abo-Dahab [20] applied the DPL theory to study magneto-thermoelastic interaction in the inhomogeneous body with a spherical cavity. Zenkour et al. [21] discussed the Seebeck effect and magneto-thermoelastic interaction in the solid cylinder when the thermal conductivity is temperature-dependent. Deswal and Kalkal [22] used the state-space method to study a two-temperature model for magneto-thermoelasticity under initial stress. Bachher and Sarkar [23] displayed a two-dimensional problem of magneto-thermoelasticity due to a conduction equation with frictional heat. Singh and Kumar [24] applied the eigenvalue method to investigate the effect of rotating on the magneto-thermoelastic micropolar body. One team of researchers who studied generalized magneto-thermodynamic equations in the general case is Nayfeh and Nemat-Nasser [25], which they studied the wave propagation in bodies due to the effect of electromagnetic fields.

In the present work, the effect of photo-thermoelastic interactions for semiconductor solid cylinder is considered. The analytical solution is gained by using the techniques of the Laplace transform. To get the solutions in the physical domain, a numerical method is employed. Some outcomes are illustrated in graphs to discuss the coupling impact between the thermoelastic, magnetic, and plasma waves.

2. Photothermal theory

In conjunction with generalized photo-thermoelasticity (GPTE) and coupled thermoelectric diffusion waves, the basic equations for a linear, homogeneous, and thermoelastic material under a magnetic field with constant intensity $\vec{H}$, take the following forms [1, 11, 13]:

The constitutive equations:

$$\sigma_{ij} = 2\mu e_{ij} + \lambda e_{ij} - \gamma\theta\delta_{ij} - d_n n\delta_{ij}, \tag{1}$$

where

$$2e_{ij} = u_{j,i} + u_{i,j}. \tag{2}$$

The equations of motion:

$$\sigma_{ji,j} + F_i = \ddot{u}_i. \tag{3}$$

The above equations after using Eq. (1) become

$$(\lambda + \mu)u_{i,ij} + \mu u_{i,jj} - \gamma\theta_{,i} - d_n n_{,i} + F_i = \ddot{u}_i. \tag{4}$$

The heat conduction equation taken into account the effect of the photoacoustic and thermal in semiconductor materials takes the form [3, 11, 13]

$$\left(K\theta_{,i}\right)_{,i} = \left(1 + \tau_0 \frac{\partial}{\partial t}\right)\left(\rho C_e \frac{\partial\theta}{\partial t} + \gamma T_0 \frac{\partial e}{\partial t} - \frac{E_g}{\tau_1} n\right). \tag{5}$$

The plasma wave equation can be written as [11, 13]

$$D_E n_{,ii} = \rho\frac{\partial n}{\partial t} + \frac{n}{\tau_1} + \frac{\kappa}{\tau}\theta. \tag{6}$$

We assumed that the adjacent free space is saturated by an initial magnetic field $\vec{H}$. This produces an induced electric field $\vec{E}$ and brought the magnetic field $\vec{h}$ that satisfies electromagnetism Maxwell's equations and is suitable for slowly moving media:

$$\vec{J} = \nabla \times \vec{h},\ \nabla \times \vec{E} = -\mu_0 \frac{\partial \vec{h}}{\partial t},\ \vec{E} = -\mu_0\left(\frac{\partial \vec{h}}{\partial t} \times \vec{H}\right),\ \nabla \cdot \vec{h} = 0, \tag{7}$$

$$\tau_{ij} = \mu_0\left[H_i h_j + H_j h_i - H_k h_k \delta_{ij}\right]. \tag{8}$$

3. Formulation of the problem

Let us consider due to symmetry, a one-dimensional problem of a thermally, homogeneous, isotropic, and electrically conducting cylinder of radius a. So, all quantities are considered to be depending on the time t and the distance r. The outer surface of the cylinder is under a periodic and decaying time-dependent varying heat and traction free. The cylindrical coordinates system (r, ξ, z) is used with z-axis lying along the axis of the cylinder. The cylinder is initially at a constant uniform temperature T_0. In addition, for the regularity, all studied fields are considered to vanish as $r \longrightarrow 0$.

The displacement vector has the components

$$u_r = u(r,t), \quad u_\xi(r,t) = u_z(r,t) = 0. \tag{9}$$

The constitutive relations that given in Eq. (1) take the form

$$\sigma_{rr} = 2\mu\frac{\partial u}{\partial r} + \lambda e - \gamma\theta - d_n n, \tag{10}$$

$$\sigma_{\xi\xi} = 2\mu\frac{u}{r} + \lambda e - \gamma\theta - d_n n, \tag{11}$$

$$\sigma_{zz} = \lambda e - \gamma\theta - d_n n, \tag{12}$$

$$\sigma_{rz} = \sigma_{r\xi} = \sigma_{\xi z} = 0, \tag{13}$$

where

$$e = \frac{1}{r}\frac{\partial(ru)}{\partial r}. \tag{14}$$

The electromagnetic dynamic equation of the solid cylinder is expressed as

$$\frac{\partial \sigma_{rr}}{\partial r}+\frac{1}{r}\left(\sigma_{rr}-\sigma_{\xi\xi}\right)+F_r=\rho\frac{\partial^2 u}{\partial t^2}. \tag{15}$$

Since the cylinder is sited in a magnetic field with a constant intensity $\vec{H}_0=(0,0,H_0)$, then from Eq. (7), we get

$$\vec{E}=\mu_0 H_0\left(0,\frac{\partial u}{\partial t},0\right),\quad \vec{J}=\left(0,\frac{\partial e}{\partial r},0\right),\quad \vec{h}=(0,0,e). \tag{16}$$

For a perfect conductor, the radial component of Lorentz force F_r brought by the magnetic field $\vec{H}_0$ is

$$F_r=\mu_0\left(\vec{J}\times\vec{H}_0\right)_r. \tag{17}$$

Thus, from Eqs. (8), (16) and (17), we get F_r and Maxwell's stress τ_{rr} in the forms

$$F_r=\mu_0 H_0^2\frac{\partial e}{\partial r},\qquad \tau_{rr}=\mu_0 H_0^2 e \tag{18}$$

From Eqs. (10), (11), (15), and (18), we obtain

$$(\lambda+2\mu+\mu_0 H_0^2)\frac{\partial e}{\partial r}-\gamma\frac{\partial \theta}{\partial r}-d_n\frac{\partial n}{\partial r}=\rho\frac{\partial^2 u}{\partial t^2}. \tag{19}$$

Applying the differential operator $\frac{1}{r}\frac{\partial}{\partial r}(r)$ to both sides of Eq. (19), we get

$$(\lambda+2\mu+\mu_0 H_0^2)\nabla^2 e-\gamma\nabla^2\theta-d_n\nabla^2 n=\rho\frac{\partial^2 e}{\partial t^2}. \tag{20}$$

In what tails we will utilize the accompanying dimensionless factors

$$\begin{gathered}\{R,U\}=c_0\eta\{r,u\},\quad \tau=c_0^2\eta t,\quad \{\Theta,N\}=\frac{1}{\rho c_0^2}\{\gamma\theta,d_{\mathrm{n}}n\},\\ \left\{\Sigma_{ij},\mathrm{M}_{rr}\right\}=\frac{\{\sigma_{ij},\tau_{rr}\}}{\rho c_0^2},\quad \eta_0=\frac{\rho C_E}{K},\quad \eta_0=\frac{\rho C_E}{K},\quad c_0^2=c_1^2+a_0^2,\end{gathered} \tag{21}$$

where $c_1=\sqrt{\frac{\lambda+2\mu}{\rho}}$ is the dilatational wave velocity in the half-space and $a_0=\sqrt{\frac{\mu_0 H_0^2}{\rho}}$ is the Alfven wave velocity of the medium. Utilizing non-dimensional factors (21), the fundamental equations take the structures

$$\nabla^2\Theta=\left(1+\tau_0\frac{\partial}{\partial t}\right)\left(\frac{\partial\Theta}{\partial \mathrm{t}}+\varepsilon_1\frac{\partial E}{\partial t}-\varepsilon_1 N\right), \tag{22}$$

$$\nabla^2 E-\nabla^2\Theta-\nabla^2 N=\frac{\partial^2 E}{\partial\tau^2}, \tag{23}$$

$$\nabla^2 N=g_1\frac{\partial N}{\partial\tau}+g_2 N+g_3\Theta, \tag{24}$$

$$E=\frac{1}{R}\frac{\partial(RU)}{\partial R}, \tag{25}$$

$$\begin{gathered}\Sigma_{rr}=2\beta^2\frac{\partial U}{\partial R}+(1-2\beta^2)E-\Theta-N,\\ \Sigma_{\xi\xi}=2\beta^2\frac{U}{R}+(1-2\beta^2)E-\Theta-N,\\ \Sigma_{zz}=(1-2\beta^2)E-\Theta-N,\end{gathered} \tag{26}$$

where

$$\begin{gathered}\beta^2=\frac{\mu}{\lambda+2\mu},\quad \varepsilon_1=\frac{\gamma^2 T_0}{\rho^2 C_e c_0^2},\quad \varepsilon_2=\frac{\gamma E_g c_0^2}{\tau d_{n\rho} C_e},\quad E=\frac{1}{R}\frac{\partial(RU)}{\partial R},\\ g_1=\frac{\rho}{D_E\eta},\quad g_2=\frac{1}{D_E\eta_0\tau_1},\quad g_3=\frac{\kappa d_n}{\gamma D_E\eta_0^2}.\end{gathered}$$

4. Initial and boundary conditions

Here we can express the initial conditions of the problem as

$$U(R,0)=\frac{\partial U(R,0)}{\partial R}=0,\quad N(R,0)=\frac{\partial N(R,0)}{\partial R}=0,$$
$$\Theta(R,0)=\frac{\partial \Theta(R,0)}{\partial R}=0. \tag{27}$$

We guess that the boundary of the cylinder $R=a$ is compelled and is exposed to a heat fluctuating which periodically and decaying. So the accompanying boundary conditions are held:

- The surface of the cylinder is exposed to a sinusoidal and decaying varying heat

$$\Theta(a,\tau)=\Theta_0\,\tau\,\mathrm{e}^{-\tau/2}\cos(\omega\tau),\ \ \omega>0, \tag{28}$$

where and Θ_0 is constant and ω is a temperature frequency.

- The mechanical boundary condition as the displacement of the surface is constrained in the form

$$U(a,\tau)=0. \tag{29}$$

During the diffusion procedure, the carriers can arrive at the surface of the sample with a limited likelihood of recombination. Then the limit state of carrier density can be summarized below:

$$D_E\frac{\partial N(a,\tau)}{\partial R}=s_v N(a,\tau), \tag{30}$$

where s_v is the surface recombination velocity.

5. Laplace transforms domain

Laplace transform is taken for Eqs. (22)-(26), under the homogeneous initial conditions (22), one gets:

$$\nabla^2\bar{\Theta}=q(s\bar{\Theta}+s\varepsilon_1\bar{E}-\varepsilon_2\bar{N}), \tag{31}$$
$$\nabla^2\bar{E}-\nabla^2\bar{\Theta}-\nabla^2\bar{N}=s^2\bar{E}, \tag{32}$$
$$\nabla^2\bar{N}=sg_1\bar{N}+g_2\bar{N}+g_3\bar{\Theta}, \tag{33}$$
$$\bar{\Sigma}_{rr}=2\beta^2\frac{\partial\bar{U}}{\partial R}+(1-2\beta^2)\bar{E}-\bar{\Theta}-\bar{N},$$
$$\bar{\Sigma}_{\xi\xi}=2\beta^2\frac{\bar{U}}{R}+(1-2\beta^2)\bar{E}-\bar{\Theta}-\bar{N}, \tag{34}$$
$$\bar{\Sigma}_{zz}=(1-2\beta^2)\bar{E}-\bar{\Theta}-\bar{N},$$

where $q=(1+\tau_0 s)$.

Eliminating $\bar{\Theta}$, $\bar{N}$ or $\bar{E}$ from Eqs. (31)-(33), one gets

$$(\nabla^6-A\nabla^4+B\nabla^2-C)\{\bar{\Theta},\bar{N},\bar{E}\}=0, \tag{35}$$

where the coefficients A, B, and C are given by

$$A=s^2+g_5-\frac{g_7}{g_3},\quad B=s^2g_5+g_6+\frac{g_7(g_4-g_3)}{g_3},\quad C=s^2g_6, \tag{36}$$

where

$$g_4=sg_1+g_2,\quad g_5=qs+g_5,\quad g_6=qs\,g_4+\,g_3q\varepsilon_2,\quad g_7=g_3sq\varepsilon_1. \tag{37}$$

Presenting m_i, $(i=1,2,3)$ into Eq. (35), one obtains

$$(\nabla^2-m_1^2)(\nabla^2-m_2^2)(\nabla^2-m_3^2)\{\bar{\Theta},\bar{N},\bar{E}\}=0, \tag{38}$$

where m_1^2, m_2^2 and m_3^2 are the roots of

$$m^6-Am^3+Bm^2-C=0. \tag{39}$$

These roots are given by

$$m_1^2 = \frac{1}{3}[2p_0 \sin q_0 + A],$$
$$m_2^2 = -\frac{1}{3}p_0\left[\sin q_0 + \sqrt{3}\cos q_0\right] + \frac{1}{3}A,$$
$$m_2^2 = \frac{1}{3}p_0\left[\sqrt{3}\cos q_0 - \sin q_0\ \right] + \frac{1}{3}A,$$

where

$$p_0 = \sqrt{A^2 - 3B}, \quad q_0 = \frac{1}{3}\sin^{-1}\left(-\frac{2A^3 - 9AB + 27C}{2p_0^3}\right).$$

The solutions of Eq. (38) is expressed as

$$\bar{E} = \sum_{i=1}^{3} A_i I_0(m_i R), \tag{40}$$

where $I_0(\ .\ )$ is the modified Bessel's function of the second kind of order zero and A_i, $(i = 1,2,3)$ are some parameters in terms of *s*. In the same manner, one obtains

$$\{\bar{\theta}, \bar{N}\} = \sum_{i=1}^{3}\{L_n, M_n\}A_i I_0(m_i R), \tag{41}$$

where $\boldsymbol{L_n}$ and $\boldsymbol{M_n}$ are different parameters related to $\boldsymbol{A_i}$. Substituting Eqs. (40) and (41) into Eqs. (31) and (32), we obtain the relations:

$$M_n = \frac{g_7}{k_n^4 - g_5 k_n^2 + g_6}, \quad L_n = \frac{g_7(k_n^2 - g_4)}{g_3(k_n^4 - g_5 k_n^2 + g_6)}.$$

In Laplace transform domain, from Eqs. (25) and (40), one gets

$$\bar{U} = \sum_{i=1}^{3} \frac{1}{m_i} A_i I_1(m_i R). \tag{42}$$

To derive Eq. (42), one used the well-known relation of Bessel's function as

$$\int x\, I_0(x)dx = xI_1(x). \tag{43}$$

Differentiating Eq. (43) concerning R, we get

$$\frac{\partial \bar{U}}{\partial R} = \sum_{i=1}^{3} A_i \left[I_0(m_i R) - \frac{1}{R\, m_i} I_1(m_i R)\right]. \tag{44}$$

Thus from Eqs. (40), (41), (42), (43) and (34) it can be obtained

$$\begin{aligned} \bar{\Sigma}_{rr} &= \sum_{i=1}^{3} A_i \left[R_n I_0(m_i R) - \frac{2\beta^2}{R\, m_i} I_1(m_i R)\right], \\ \bar{\Sigma}_{\xi\xi} &= \sum_{i=1}^{3} A_i \left[Q_n I_0(m_i R) + \frac{2\beta^2}{R\, m_i} I_1(m_i R)\right], \\ \bar{\Sigma}_{zz} &= \sum_{i=1}^{3} A_i Q_n I_0(m_i R)\,, \end{aligned} \tag{45}$$

where

$$R_n = 1 - L_n - H_n, \quad Q_n = 1 - 2\beta^2 - L_n - H_n.$$

The non-dimensional Maxwell's stress M_{rr} is given by

$$\mathrm{M}_{rr} = \frac{a_0^2}{c_0^2} e = \frac{a_0^2}{c_0^2}\sum_{i=1}^{3} A_i I_0(m_i R). \tag{46}$$

After applying the Laplace transform, the boundary conditions (28)-(30) take the forms

$$\begin{aligned} \bar{\theta} &= \frac{4\Theta_0(1 + 4s + 4s^2 - 4\omega^2)}{(1 + 4s + 4s^2 + 4\omega^2)^2} = \bar{G}(s), \\ \bar{U}(a, s) &= 0, \\ D_E \left.\frac{\partial \bar{N}(a,s)}{\partial R}\right|_{R=a} &= s_f \bar{N}(a, s). \end{aligned} \tag{47}$$

Substituting Eqs. (35)-(37) into (41), one obtains

$$\begin{gathered}\sum_{i=1}^{3} A_i I_0(a\, m_i) = \bar{G}(s),\\ \sum_{i=1}^{3} \frac{1}{m_i} A_i I_1(a\, m_i R) = 0\,,\\ \sum_{i=1}^{3} A_i M_i \left[(D_E - s_v) I_0(m_i a) - \frac{D_E}{a\, m_i} I_1(m_i a)\right] = 0.\end{gathered} \tag{48}$$

Solving the system (42), one gets the estimations of constants, A_i, $(i = 1,2,3)$. Here, a precise and proficient numerical strategy dependent on a Fourier series expansion [25] is utilized to acquire the inversion of the Laplace transforms. In this strategy, any function in Laplace space can be altered to the time domain as

$$\Gamma(R,\tau) = \frac{e^{c\tau}}{\tau}\left[\frac{1}{2}\bar{\Gamma}(R,c) + \mathrm{Re}\sum_{n=1}^{N_f} \bar{\Gamma}\left(R, c + \frac{in\pi}{\tau}\right)(-1)^n\right], \tag{49}$$

where N_f is a limited number of terms, Re is the real part, i is an imaginary number unit and c fulfills the connection $c\tau \cong 4.7$ [26].

6. Numerical results

In this section, some numerical results have been computed numerically. The physical parameters used in the calculations are given at $T_0 = 298$ K as follows [11]:

$$\lambda = 2.696 \times 10^{10}\,\mathrm{kg\,m^{-1}s^{-2}},\ \ \mu = 1.639 \times 10^{10}\,\mathrm{kg\,m^{-1}s^{-2}},\ \ \rho = 1740\,\mathrm{kg\,m^{-3}},$$
$$K = 2.510\,\mathrm{W\,m^{-1}K^{-1}},\ \ C_E = 1.04 \times 10^{3}\,\mathrm{J\,kg\,K^{-1}},\ \ d_n = -9 \times 10^{-31}\,\mathrm{m^3},$$
$$E_g = 1.11\,\mathrm{eV},\ \ D_E = 2.5 \times 10^{-3}\,\mathrm{m^2\,s^{-1}},\ \ s_f = 2\,\mathrm{m\,s^{-1}},\ \ \tau = 5 \times 10^{-5}\,\mathrm{s}.$$

With the help of these physical values, under the generalized theoretical modeling of photo-thermoelasticity (GPTE), the values of the non-dimensional temperature Θ, displacement U, thermal stresses Σ_{rr} and $\Sigma_{\xi\xi}$, Maxwell's stress M_{rr} and the absolute carrier density N (carrier density above equilibrium carrier density) are computed for the time $\tau = 0.1$ and $R = 1$. The obtained results are illustrated graphically in Figures 1–24. Numerical estimations for all field quantities are carried out in four cases as follows:

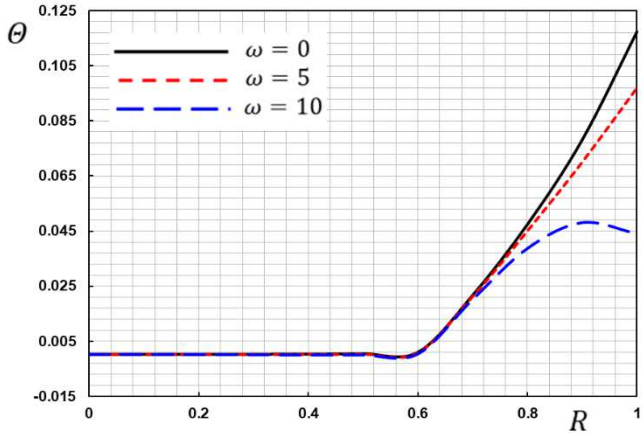

Figure 1. Variation of temperature Θ with radius R for different values of temperature frequency ω.

6.1 Case I: The effect of periodic frequency

In this case, all the studied physical field quantities with radial direction R are displayed in Figs. (1-6) for different values of the periodic frequency ω. The other physical parameters remain constant. For a thermal shock problem, $\omega = 0$, and when the cylinder is due to a decaying varying heat we set $\omega = 5{,}10$. Figs 1-6 illustrate that:

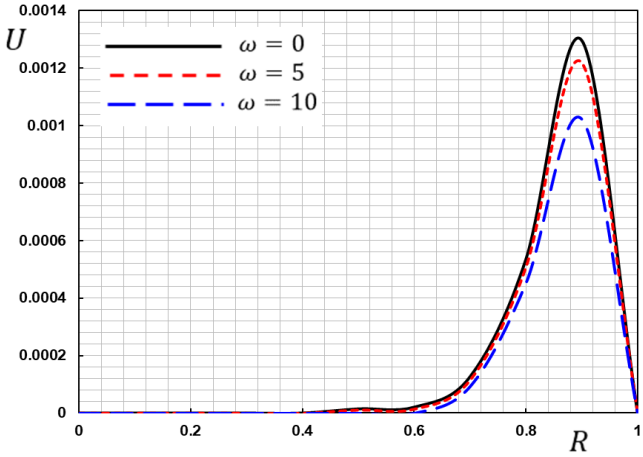

Figure 2. Variation of displacement U with radius R for different values of temperature frequency ω.

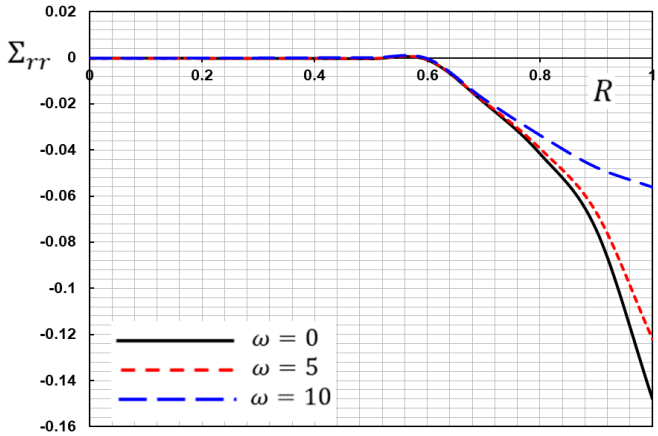

Figure 3. Variation of the stress Σ_{rr} with radius R for different values of temperature frequency ω.

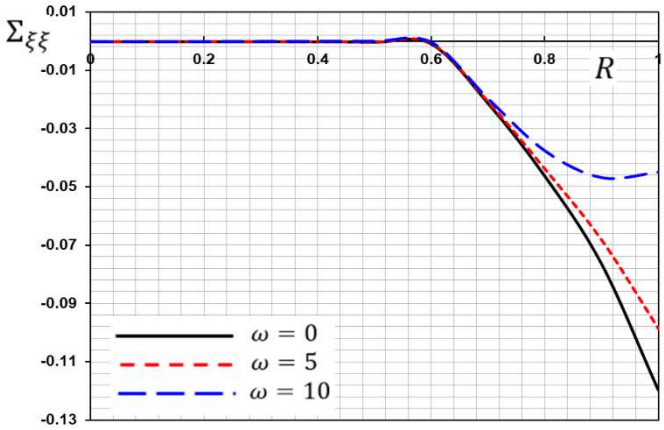

Figure 4. Variation of the stress $\Sigma_{\xi\xi}$ with radius R for different values of temperature frequency ω.

- The maximum values occur near the surface of the cylinder and their magnitudes decrease as $R \to 0$.
- The periodic frequency ω has a clear effect on the studied fields.
- The temperature Θ starts at the highest values at the surface of the cylinder due to the presence of decaying and periodic temperature and then its values gradually decrease in the opposite of increasing the radius R.
- The distribution of heat when $\omega = 5{,}10$ is less than in the case of $\omega = 0$.

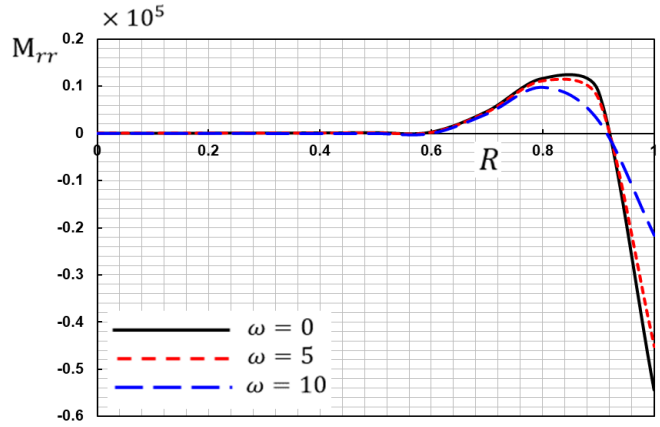

Figure 5. Variation of Maxwell's stress M_{rr} with radius R for different values of temperature frequency ω.

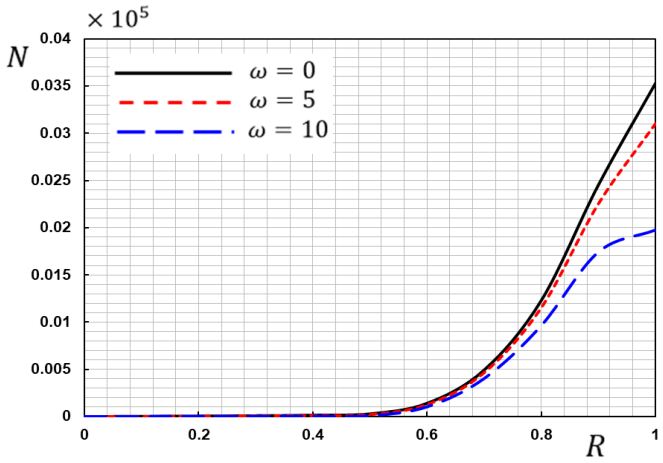

Figure 6. Variation of carrier density N with radius R for different values of fractional parameter order α.

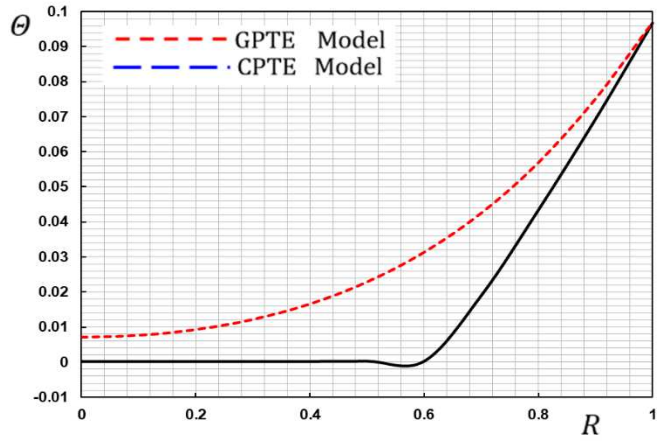

Figure 7. Variation of temperature Θ with radius R for different models of photo-thermoelasticity.

- Displacement distribution U is increasing in $0.9 \leq \Theta \leq 1$ and rapidly decreases in the interval $0.9 \leq \Theta \leq 0.6$ until it approaches zero.
- The values of displacement decrease with increasing the parameter ω.
- Stress Σ_{rr} starts at the negative value and increases rapidly until it approaches zero.
- By increasing the angular frequency values, stress Σ_{rr} values decrease.
- The second thermal stress $\Sigma_{\xi\xi}$ is the same behavior as the stress Σ_{rr}.

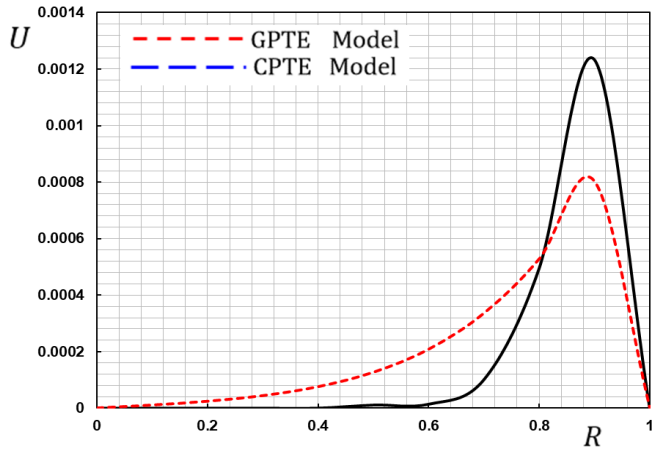

Figure 8. Variation of displacement U with radius R for different models of photo-thermoelasticity.

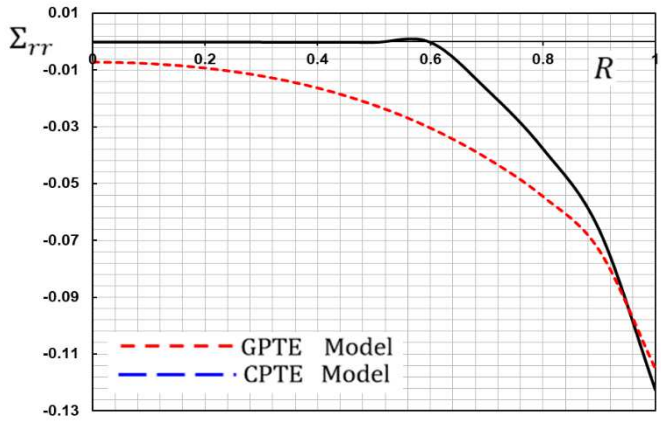

Figure 9. Variation of the stress Σ_{rr} with radius R for different models of photo-thermoelasticity.

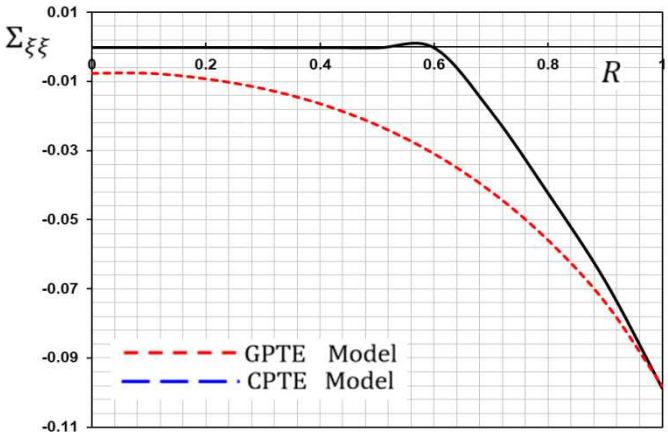

Figure 10. Variation of the stress $\Sigma_{\xi\xi}$ with radius R for different models of photo-thermoelasticity.

- Maxwell's stress M_{rr} increasing in $0.85 \leq \Theta \leq 1$ and rapidly decreases in the interval $0.85 \leq \Theta \leq 0.6$ until it approaches zero
- Like most previous distributions, carrier density N starts with the greatest value at the surface and gradually decreases until it approaches zero, which is physically consistent.
- In generalized photo-thermoelasticity with relaxation time (GPTE) the thermoelastic and plasma waves propagate with infinite speeds.

- Finally, the field quantities depend not only on the state and space variables τ and R, but also depend on the parameter of temperature frequency.

6.2 Case II: The effect of relaxation time

In the second case (Figs. (7-12)), two different values of relaxation time τ_0 are considered. two different models of thermoelasticity can be reached as special cases of the existing photo-thermoelasticity with phase lags model. The classical coupled model of photo-thermoelasticity (CPTE) introduced by Todorović [13, 14] can be obtained can be attained as special cases of the current photo-thermoelasticity (GPTE) by taking $\tau_0 = 0$. Figs. 7-12 represent variation in the values of temperature Θ, the displacement U, Maxwell's stress M_{rr}, the thermal stresses stress Σ_{rr} and $\Sigma_{\xi\xi}$ and the absolute carrier density N against the radial distance R, $(0 \leq R \leq 1)$ for $\omega = 5$ and $\tau = 0.12$. It can be observed that:

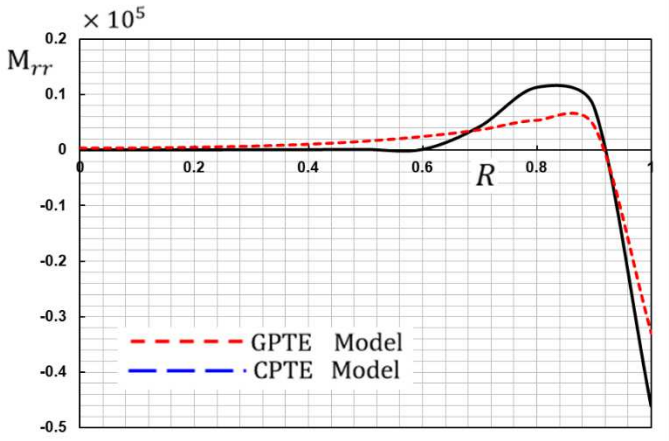

Figure 11. Variation of Maxwell's stress M_{rr} with radius R for different models of photo-thermoelasticity.

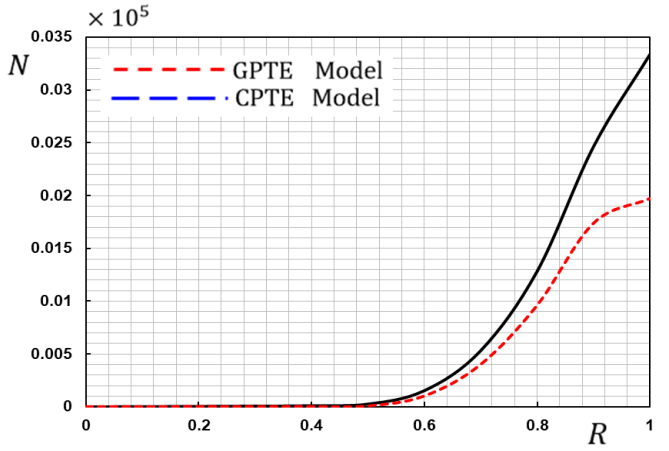

Figure 12. Variation of carrier density N with radius R for different models of photo-thermoelasticity.

- The relaxation time parameter τ_0 has a great effect on all different distributions.
- The mechanical distributions indicate that their waves propagate as waves with finite velocities.
- The values in the classical model of photo-thermoelasticity (CPTE) are different compared to those of the GPTE model
- The behavior of the two models, in general, is not similar.

- In the case of the GPTE model, thermal and optical waves are propagated with finite velocities on the contrary, in the case of the CPTE model propagating at unlimited speeds. Also, this phenomenon is clear in all figures of various studied physical functions.

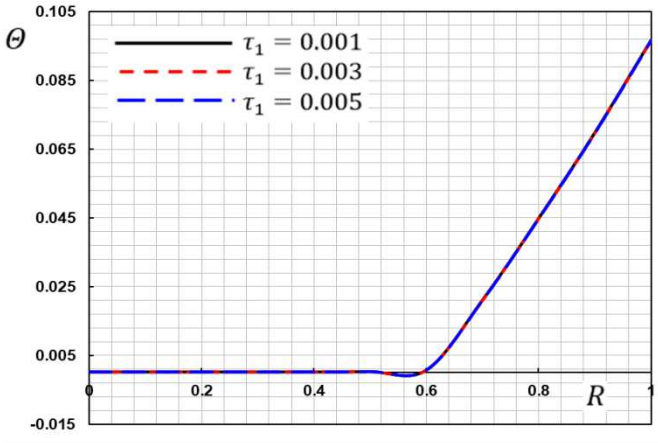

Figure 13. Variation of temperature Θ with radius R for different models of photo-thermoelasticity.

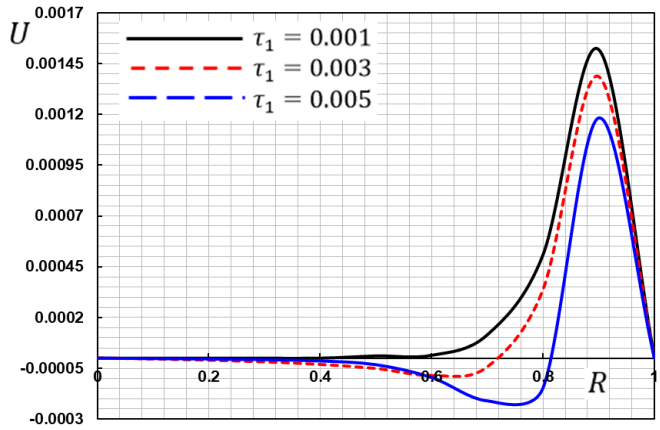

Figure 14. Variation of displacement U with radius R for different models of photo-thermoelasticity.

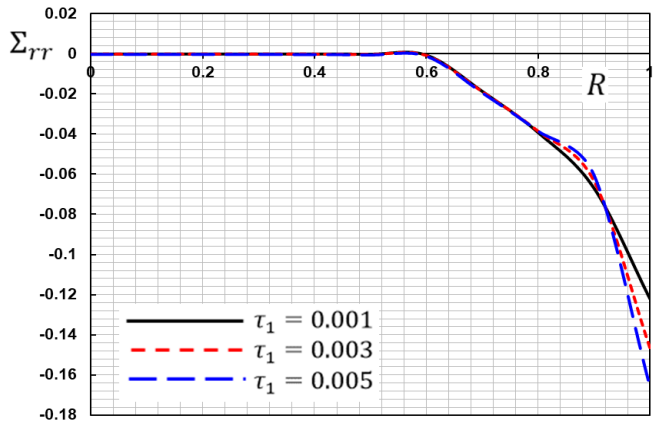

Figure 15. Variation of the stress Σ_{rr} with radius R for different models of photo-thermoelasticity.

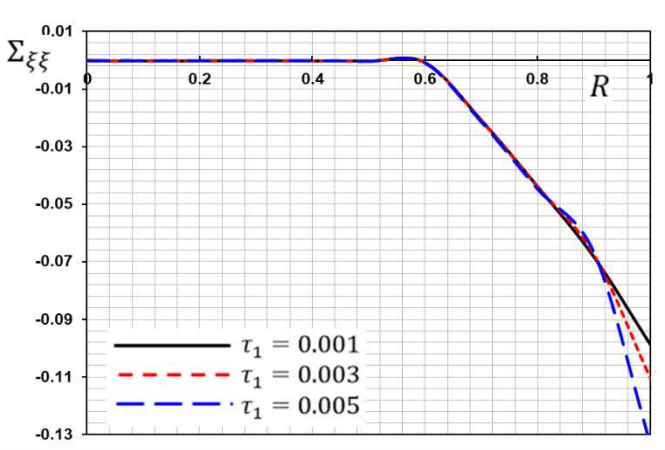

Figure 16. Variation of the stress $\Sigma_{\xi\xi}$ with radius R for different models of photo-thermoelasticity.

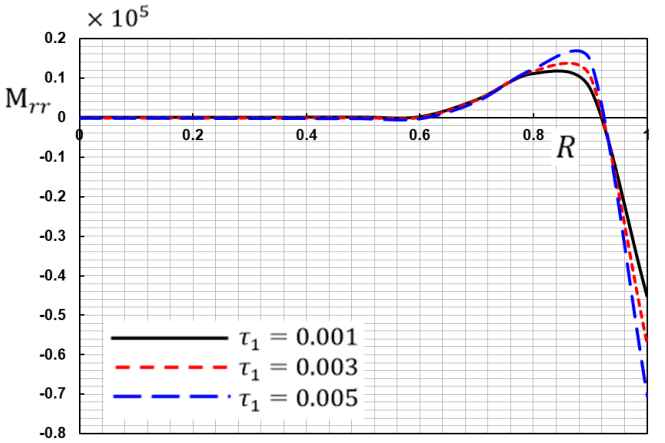

Figure 17. Variation of Maxwell's stress M_{rr} with radius R for different models of photo-thermoelasticity.

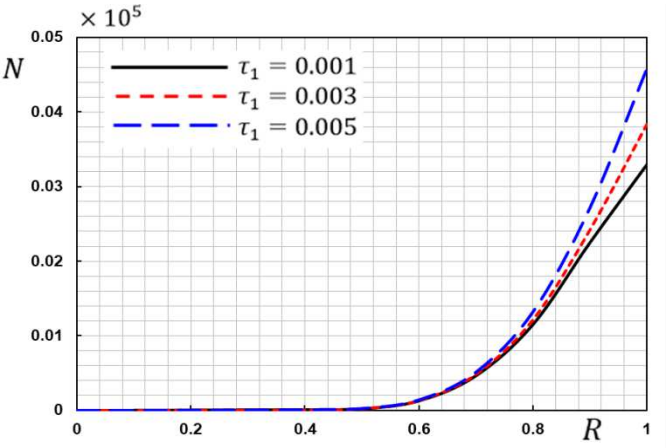

Figure 18. Variation of carrier density N with radius R for different models of photo-thermoelasticity.

6.3 Case III: Influence of the photo-generated carrier lifetime parameter

The distributions of temperature Θ, the displacement U, the thermal stresses Σ_{rr} and $\Sigma_{\xi\xi}$, Maxwell's stress M_{rr} and the absolute carrier density N due to the influence of the photo-generated carrier lifetime parameter τ_1 with distance, x are shown in Figs. 13-18. It is detected that the parameter of carrier lifetime τ_1 has significant impacts on all variables. We notice that:

- The carrier lifetime parameter does not have a clear effect on the distribution of heat Θ inside the solid cylinder.
- The parameter τ_1 has a distinct effect on the distributions of displacement U and carrier density N, especially near the surface of the cylinder.
- Carrier density distribution N increases with increasing lifetime and this is also evident from the basic equations as the N depends on τ_1 significantly (see Eq. 6).
- There is a great similarity in the dependence of stresses on the parameter τ_1 near the surface of the cylinder.
- Maxwell's stress M_{rr} increases with increasing time in some intervals and decreases in other intervals.

6.4 Case IV: Effects of time instant on the distributions

Figures 19-24 show the 3D curves to discuss the distributions of displacements, temperature change, stress forces, and carrier charge density with variations of distance R and instant time τ. We can see that the instant time τ has significant impacts on all the studied fields. It has been observed that τ to play a vital role in the development of temperature, stresses, carrier charge density, and displacement fields.

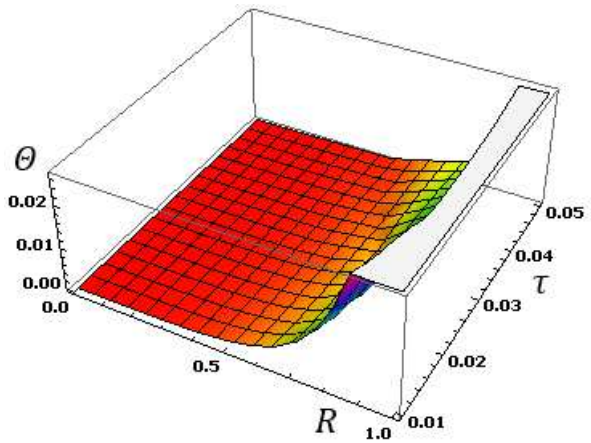

Figure 19. Variation of the temperature Θ with radius R and time τ.

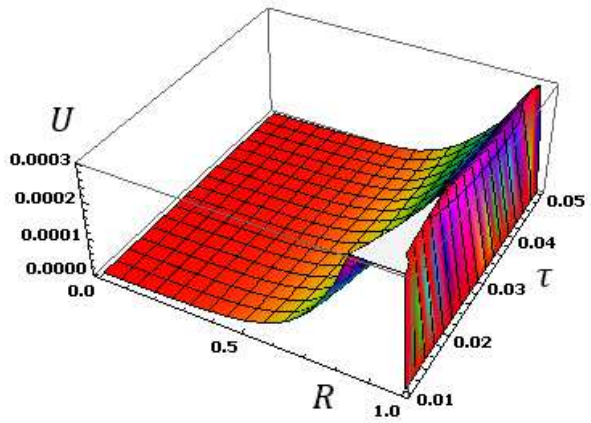

Figure 20. Variation of the displacement U with radius R and time τ.

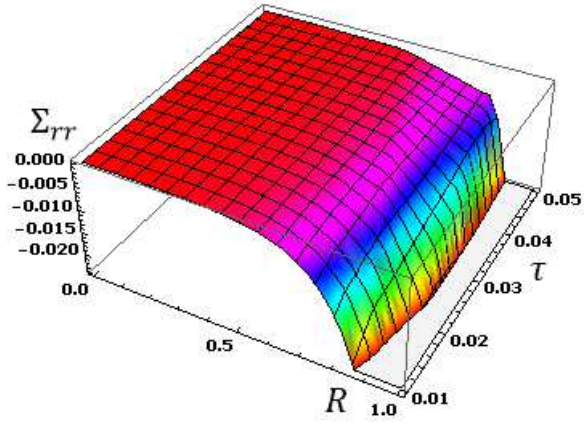

Figure 21. Variation of the stress Σ_{rr} with radius R and time τ.

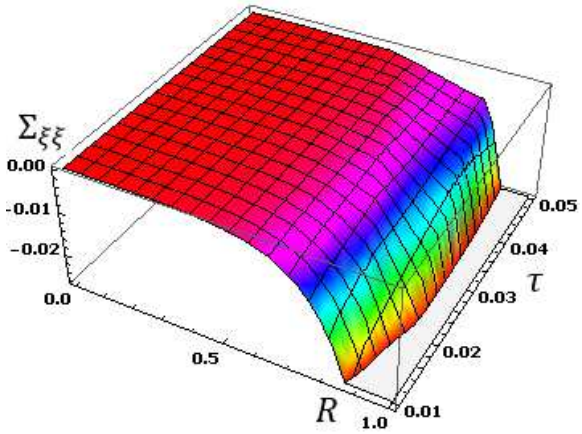

Figure 22. Variation of the stress $\Sigma_{\xi\xi}$ with radius R and time τ.

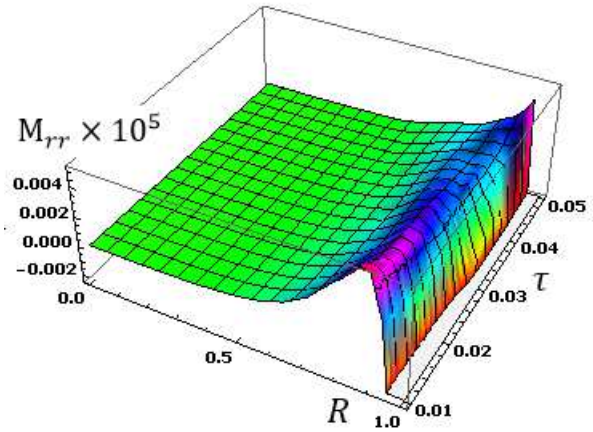

Figure 23. Variation of Maxwell's stress M_{rr} with radius R and time τ.

In these figures, it is also observed that the values of Maxwell's stress M_{rr}, displacement u, radial and hoop stresses Σ_{rr} and $\Sigma_{\xi\xi}$, temperature distribution Θ and carrier charge density N in any fixed point (R, t) increase when τ increases. Figure 20 shows that displacement U gratify the boundary condition at $R = a$ and has a different response. The comparison of these figures shows the effect of instant time τ on the field variable. The field quantities depend not only on space R, but also on the time τ.

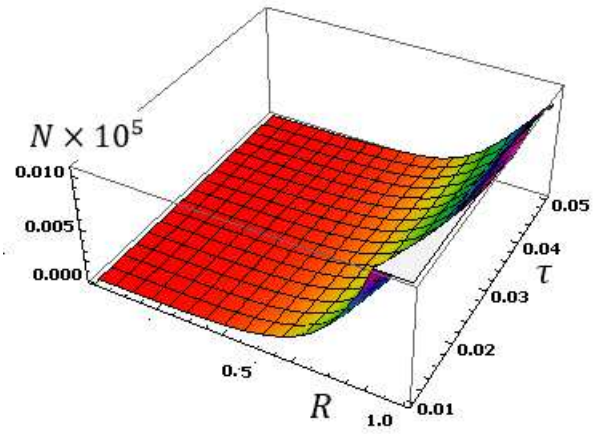

Figure 24. Variation of carrier density N with radius R and time τ.

7. Conclusions

In this article, we consider an infinitely long solid cylinder whose surface is due to a magnetic field and varying heat, and its surface traction free and constrained. We obtained the solutions using Laplace transformations and used an approximate numerical method to obtain the distributions in the physical field. From the numerical results, one can conclude that:

- The presence of photo-thermal fields has affected all the considered physical variables.
- The thermoelastic stresses, displacement, carrier charge density, and temperature have a strong dependency on the periodic frequency parameter.
- In a generalized photo-thermoelasticity model with relaxation time, heat propagates as a wave with finite velocity instead of infinite velocity in the medium.
- The relaxation time parameter has a significant effect on all the field quantities.
- The models of coupled photo-thermoelasticity CPTE can extract as a special case.
- Also, the near behavior between GPTE and PTEPL models and differs from the CPTE model that indicates the origin of the photo-thermoelastic theory.
- The results we obtained are found that they were very close to the theoretical results.
- The obtained results in this analysis should be useful to researchers who are working on a photothermal theory.
- The results presented in this work are very important for researchers, scientists, and engineers, as well as those working in the field of solid body mechanics.
- The method used in the present work applies to a wide range of problems in thermodynamics and photo-thermoelasticity.

Authors Contributions

- Conception or design of the work – Dr. A. E. Abouelregal, Dr. A. M. Zenkour.
- Data collection – Dr. A. E. Abouelregal.
- Data analysis and interpretation – Dr. A. M. Zenkour
- Drafting the article – Dr. A. E. Abouelregal
- Critical revision of the article – Dr. A. M. Zenkour

Data Availability

Not Applicable.

Funding

This research received no specific grant from any funding agency in the public, commercial, or not-for-profit sectors.

Acknowledgments

Not Applicable.

Compliance with Ethical Standards

The authors disclose that this manuscript is not submitted to any other journal and is an unpublished work.

Conflict of Interests

The authors declare that there is no conflict of interests.

Consent to Participate

Not Applicable.

Consent for Publication

As a corresponding author, I give my consent for the publication of identifiable details within the text to be published in the above Journal and Article.

References

[1] H. W. Lord and Y. Shulman, "A generalized dynamical theory of thermoelasticity", *J. Mech. Phys. Solids*, vol. 15, 299–309, 1967.
[2] E. Green and K. A. Lindsay, "Thermoelasticity", *J. Elas.*, vol. 2, pp. 1–7, 1971.
[3] D. Y. Tzou, A unified approach for heat conduction from macro- to micro-scales", *J. Heat Trans.*, vol 117, pp. 8–16, 1995.
[4] Von A. Rosencwaig, Photoacoustics and Photoacoustic Spectroscopy, Wiley: New York, 1980.
[5] A. Mandelis, M. Nestoros and C. Christofides, "Thermoelectronic-wave coupling in laser photothermal theory of semiconductors at elevated temperatures", *Opt. Eng.*, vol. 36, pp. 459–468, 1997.
[6] F. A. McDonald and G. C. Jr Wetsel, "Generalized theory of the photoacoustic effect", *J. Appl. Phys.*, vol. 49, pp. 2313–2322, 1978.
[7] M. Nestoros, B. C. Forget, C. Christofides and A. Seas, "Photothermal reflection versus temperature: quantitative analysis", *Phys. Rev. B*, vol. 51, 14115, 1995.
[8] J. Opsal and A. Rosencwaig, "Thermal and plasma wave depth profiling in silicon", *Appl. Phys. Lett.*, vol. 47, pp. 498–500, 1985.
[9] A. N. Petrovsky, A. O. Salnick, V. V. Zuev, D. O. Mukhin, M. M. Mekhtiev, J. Pelzl, A. C. Boccara and D. Fournier "Influence of carrier recombination on the pulsed photothermal beam deflection signal in semiconductors", *Solid State Commun.*, vol. 81, pp. 223–225, 1992.
[10] Y. Song, J. Bai and Z. Ren, "Reflection of plane waves in a semiconducting medium under photothermal theory", *Int. J. Thermophys.*, vol. 33, pp. 1270–1287, 2012.
[11] Y. Song, J. Bai and Z. Ren, "Study on the reflection of photothermal waves in a semiconducting medium under generalized thermoelastic theory", *Acta Mech.*, vol. 223, pp. 1545–1557, 2012.
[12] R. Stearns and G. Kino, "Effect of electronic strain on photoacoustic generation in silicon", *Appl. Phys. Lett.*, vol. 47, pp. 1048–1050, 1985.
[13] D. Todorović, "Plasma, thermal, and elastic waves in semiconductors", *Rev. Sci. Instrum.,* vol. 74, pp. 582–585, 2003.

[14] D. Todorović, "Photothermal and electronic elastic effects in microelectromechanical structures", *Rev. Sci. Instrum.*, vol. 74, pp. 578–581, 2003.
[15] L. B. Kreuzer, "Ultralow gas concentration infrared absorption spectroscopy", *J. Appl. Phys.*, vol. 42, 2934, 1971.
[16] A. M. Zenkour, "Refined two-temperature multi-phase-lags theory for thermomechanical response of microbeams using the modified couple stress analysis", *Acta Mech.*, vol. 229(9), pp. 3671–3692, 2018.
[17] A. M. Zenkour, "Refined microtemperatures multi-phase-lags theory for plane wave propagation in thermoelastic medium", *Res. Phys.*, vol. 11, pp. 929–937, 2018.
[18] A. M. Zenkour, "Refined multi-phase-lags theory for photothermal waves of a gravitated semiconducting half-space", *Compos. Struct.*, vol. 212, pp. 346–364, 2019.
[19] M. N. Allam, K. A. Elsibai, and A. E. Abouelregal, "Magnetothermoelasticity for an infinite body with a spherical cavity and variable material properties without energy dissipation", *Int. J. Solids Struct.*, vol. 47, pp. 2631–2638, 2010.
[20] A. E. Abouelregal and S. M. Abo-Dahab, "Dual phase lag model on magneto-thermoelasticity infinite non-homogeneous solid having a spherical cavity", *J. Therm. Stresses*, vol. 35, pp. 820–841, 2012.
[21] A. M. Zenkour, A. E. Abouelregal , K. A. Alnefaie and N. H. Abu-Hamdeh, "Seebeck effect on a magneto-thermoelastic long solid cylinder with temperature-dependent thermal conductivity", *Europ. J. Pure Appl. Math.*, vol. 10, pp. 786–808, 2017.
[22] S. Deswal and K. K. Kalkal, "Two temperature magneto-thermoelasticity with initial stress: state space formulation", *J. Thermodynam.*, vol. 2013, 754798, 12 pages, 2013.
[23] M. Bachher and N. Sarkar, "Two-dimensional thermal shock problem of generalized magneto-thermoelasticity with a time-fractional heat conduction law", *J. Mol. Eng. Mater.*, vol. 4, 1650004, 12 pages, 2016.
[24] R. Singh and V. Kumar, "Eigen value approach to two dimensional problem in generalized magneto micropolar thermoelastic medium with rotation effect", *Int. J. Appl. Mech. Eng.*, vol. 21, pp. 205–219, 2016.
[25] G. Honig and U. Hirdes, "A method for the numerical inversion of Laplace transform", *J. Comp. Appl. Math.*, vol. 10, pp. 113–132, 1984.
[26] D. Y. Tzou, Macro to micro-scale heat transfer: The Lagging behavior, Taylor and Francis, Washington DC: 1996.

Figures

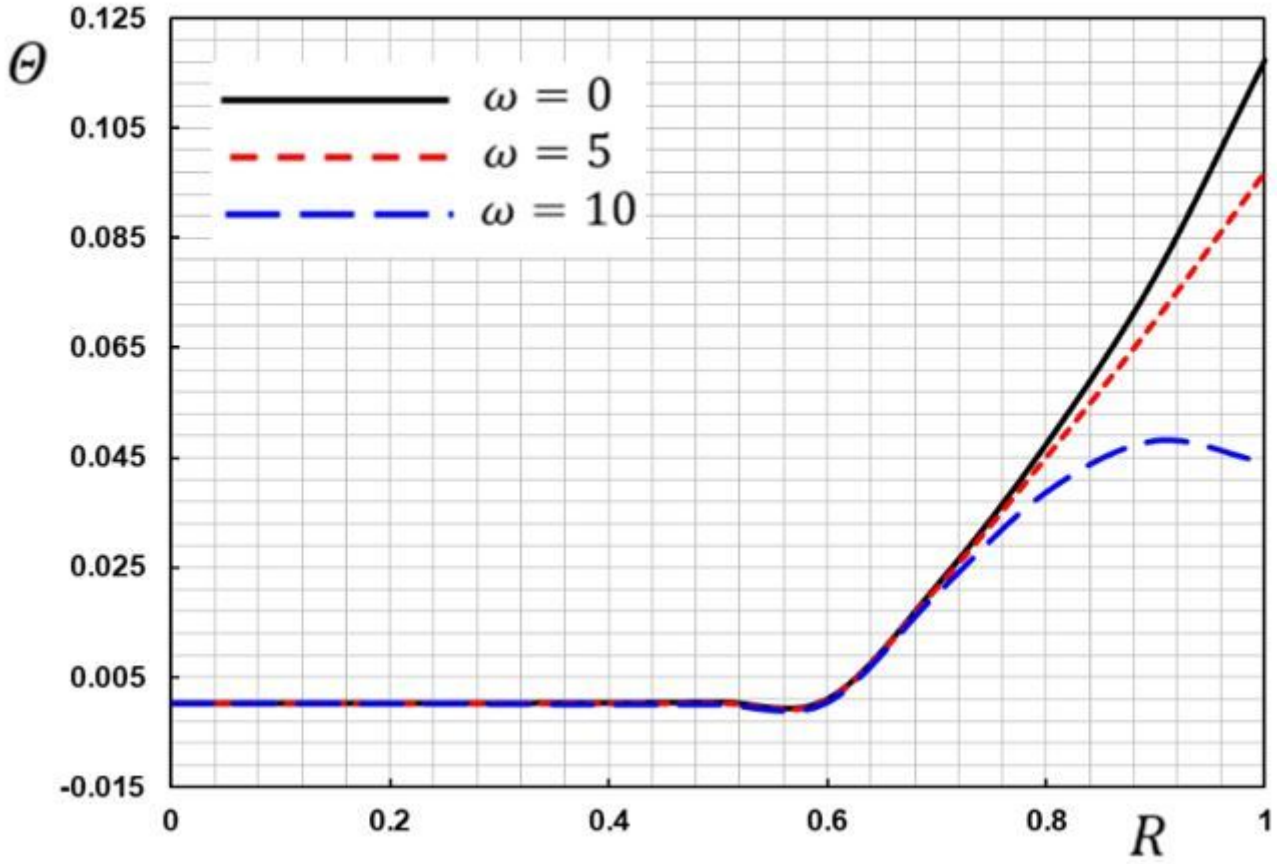

Figure 1

Variation of temperature Θ with radius R for different values of temperature frequency ω.

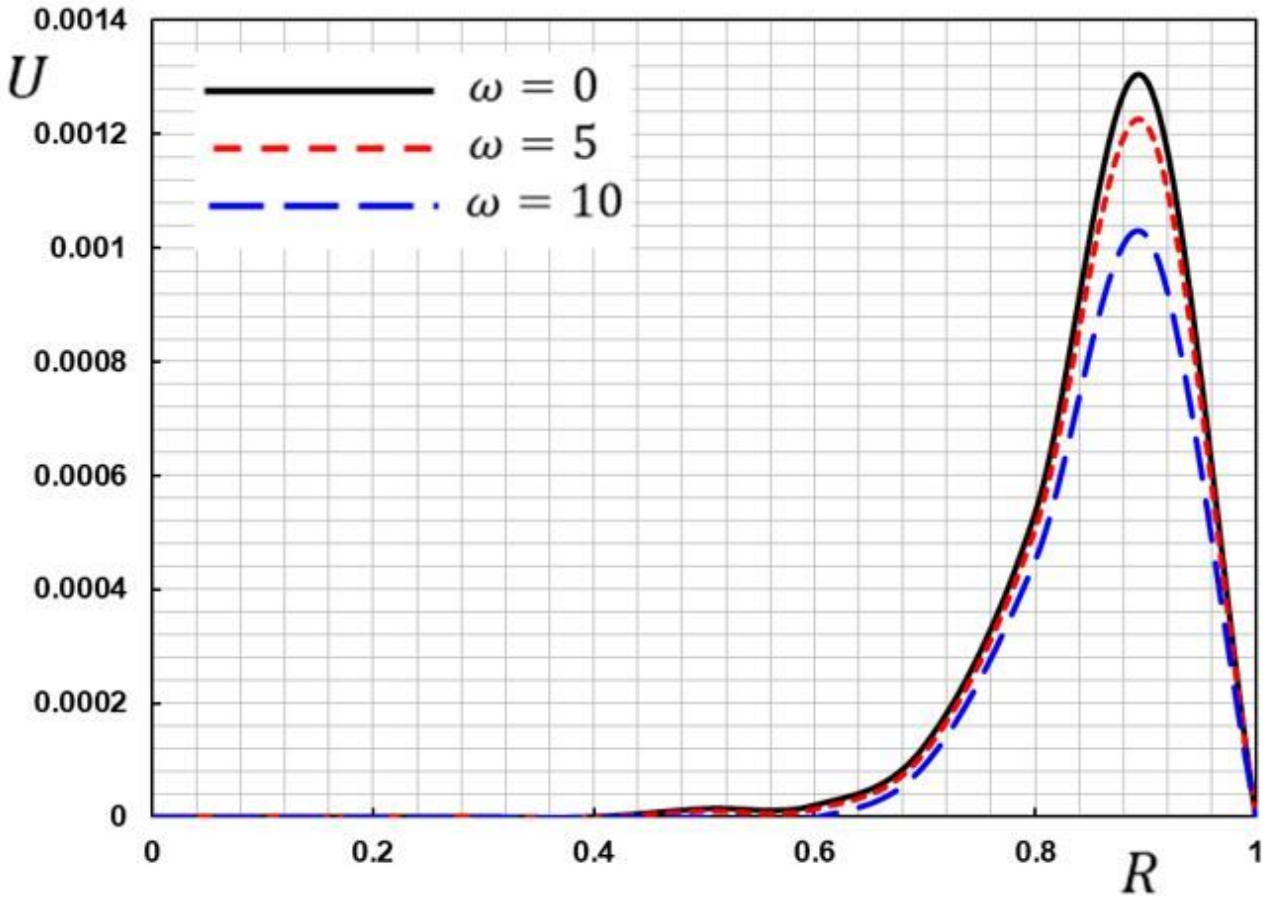

Figure 2

Variation of displacement U with radius R for different values of temperature frequency ω.

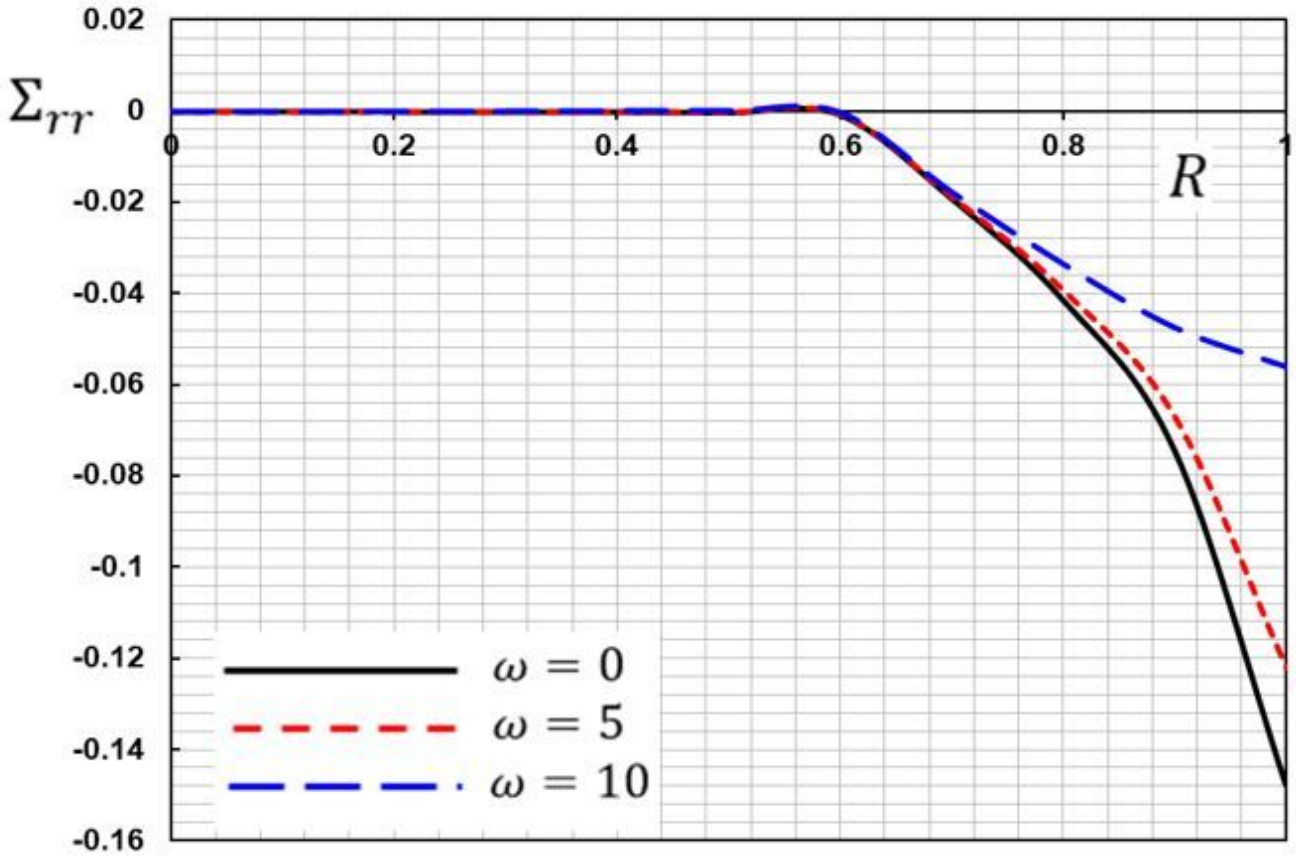

Figure 3

Variation of the stress Σ_rr with radius R for different values of temperature frequency ω.

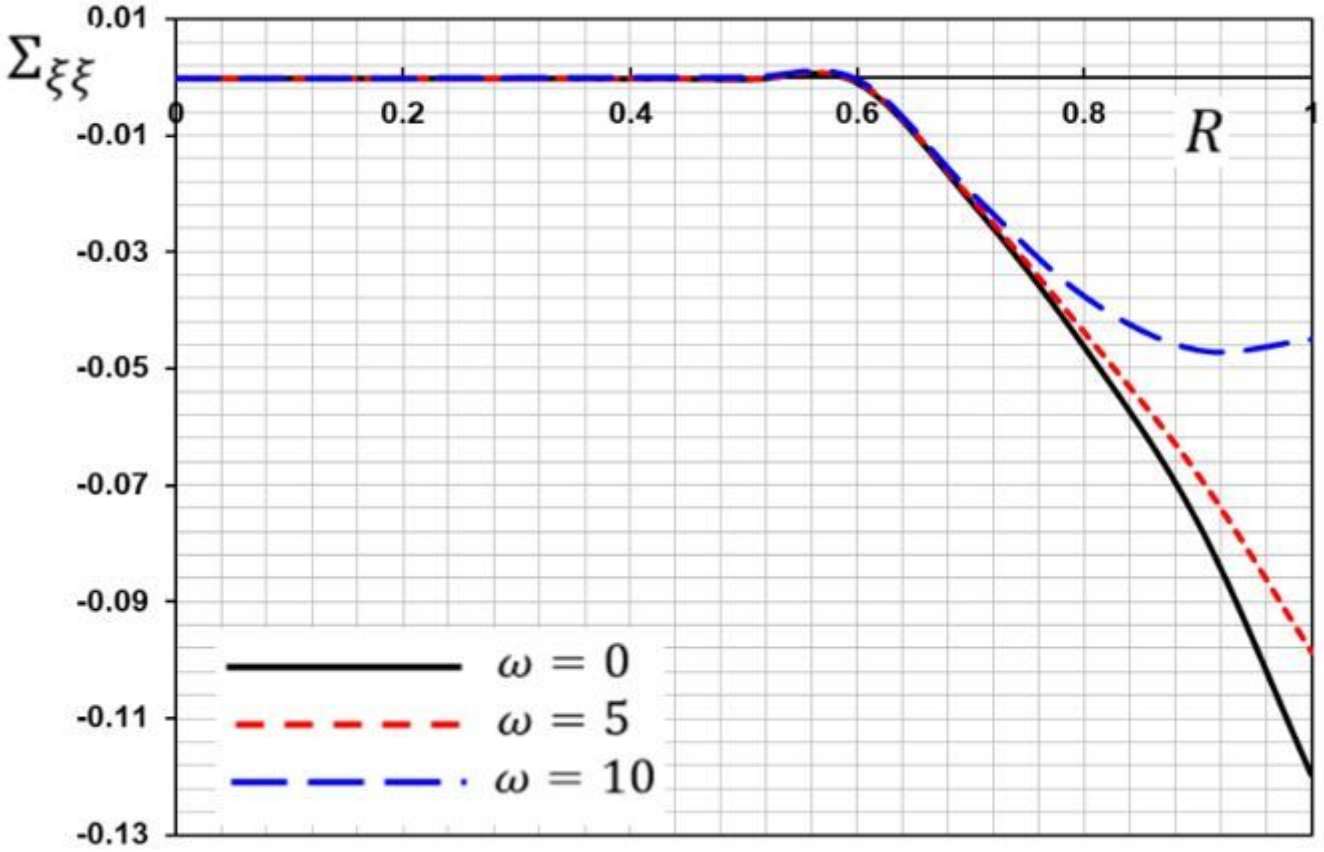

Figure 4

Variation of the stress Σ_ξξ with radius R for different values of temperature frequency ω.

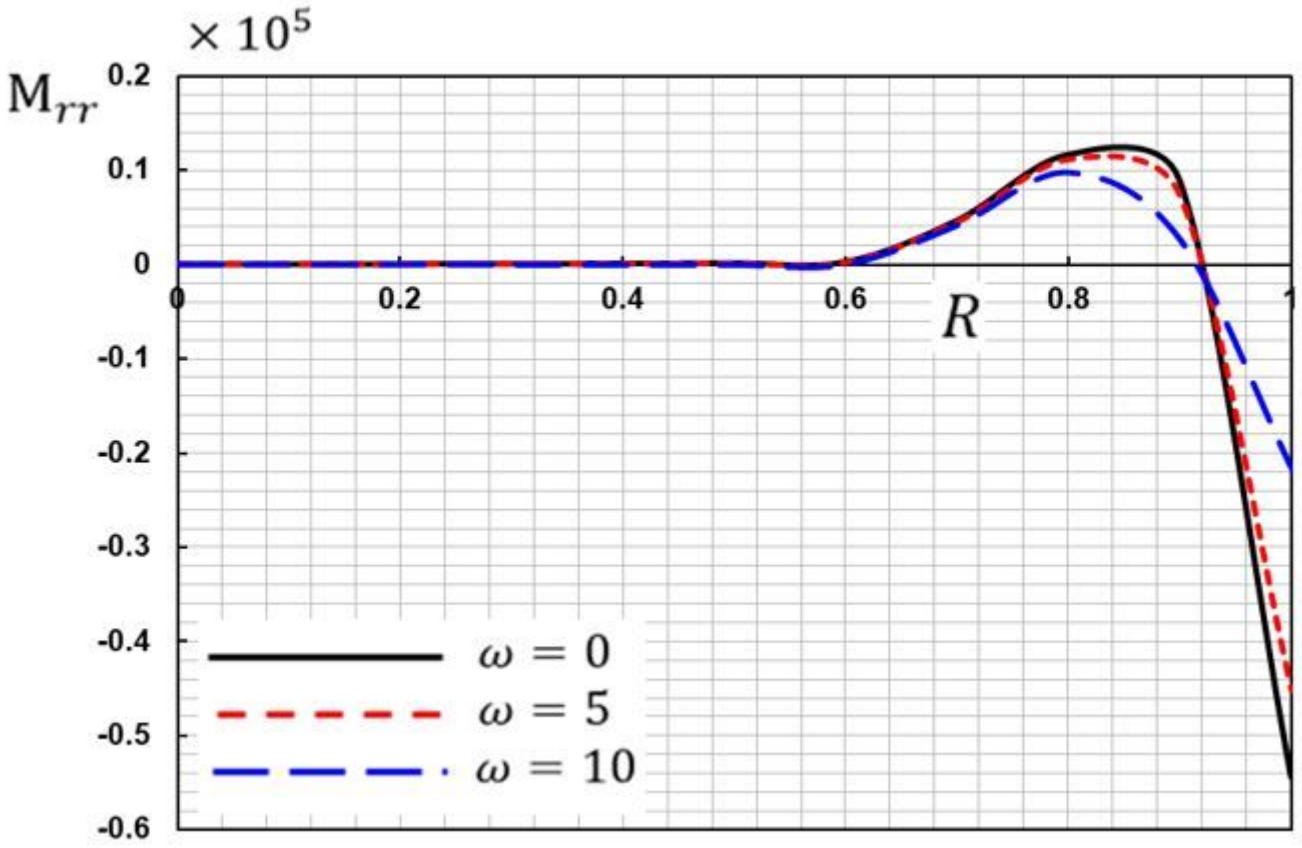

Figure 5

Variation of Maxwell's stress M_rr with radius R for different values of temperature frequency ω.

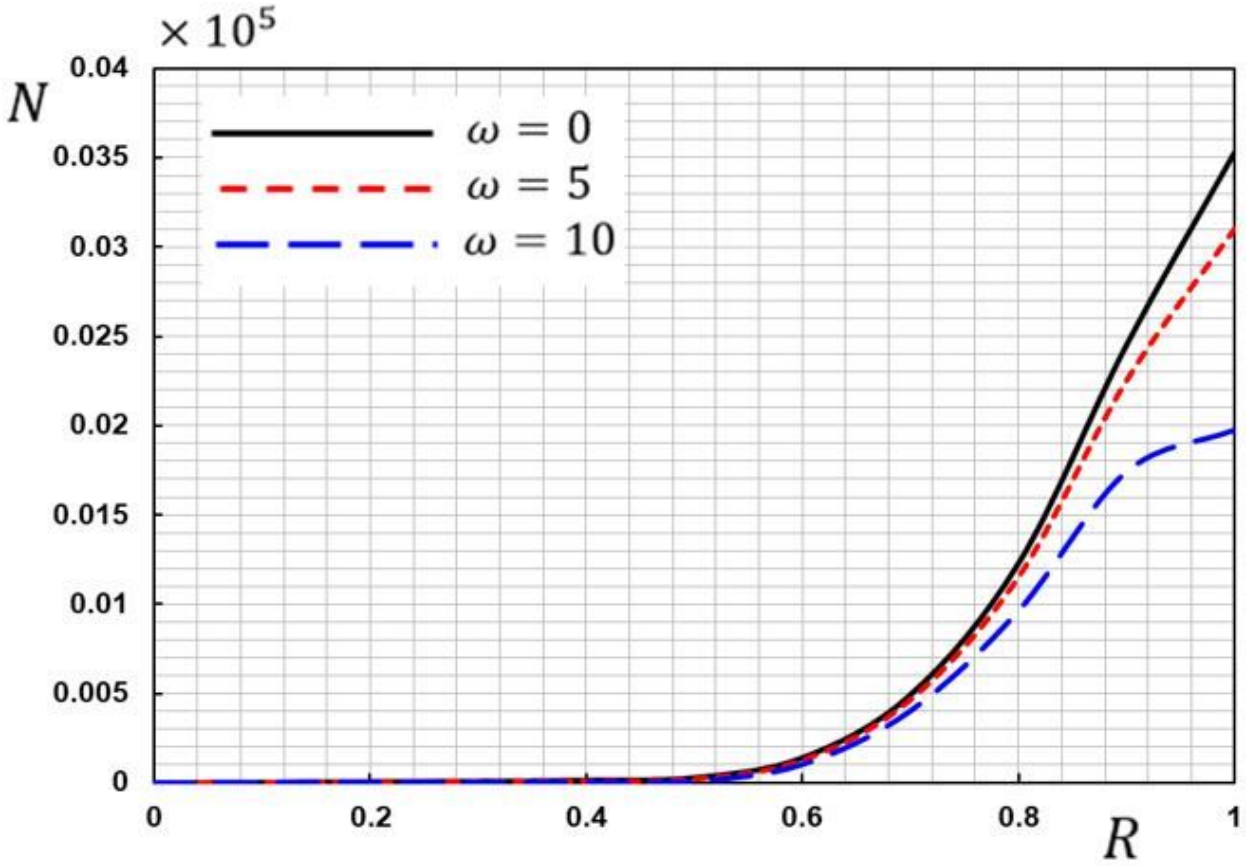

Figure 6

Variation of carrier density N with radius R for different values of fractional parameter order α.

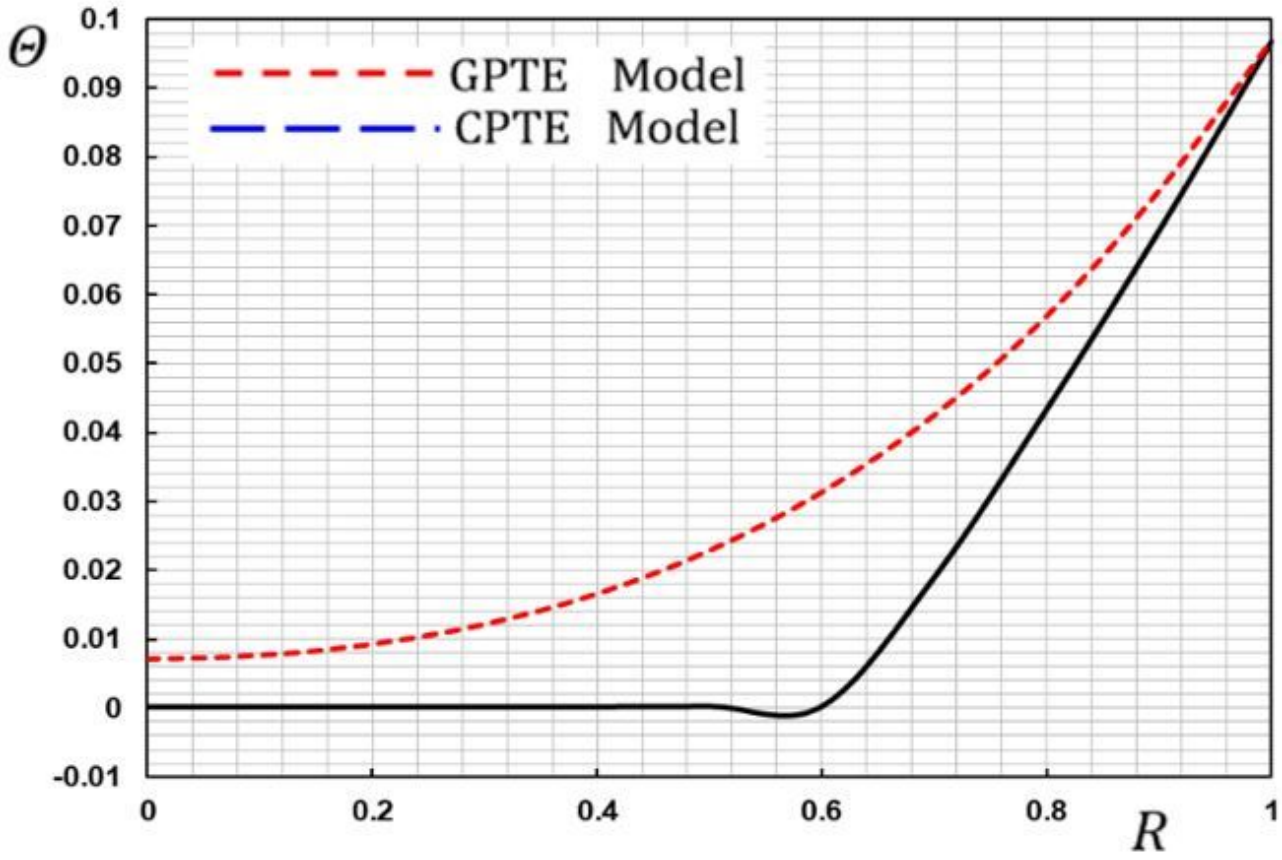

Figure 7

Variation of temperature Θ with radius R for different models of photo-thermoelasticity.

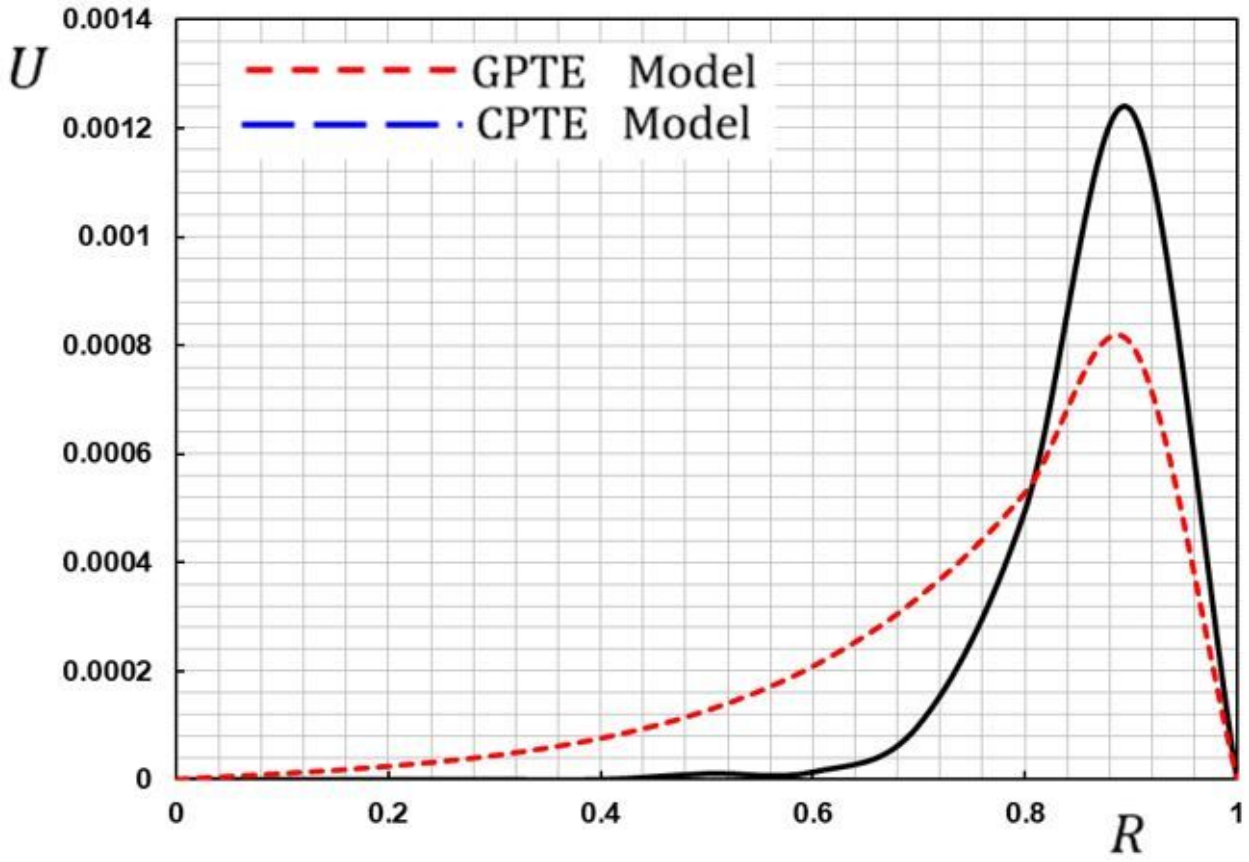

Figure 8

Variation of displacement U with radius R for different models of photo-thermoelasticity.

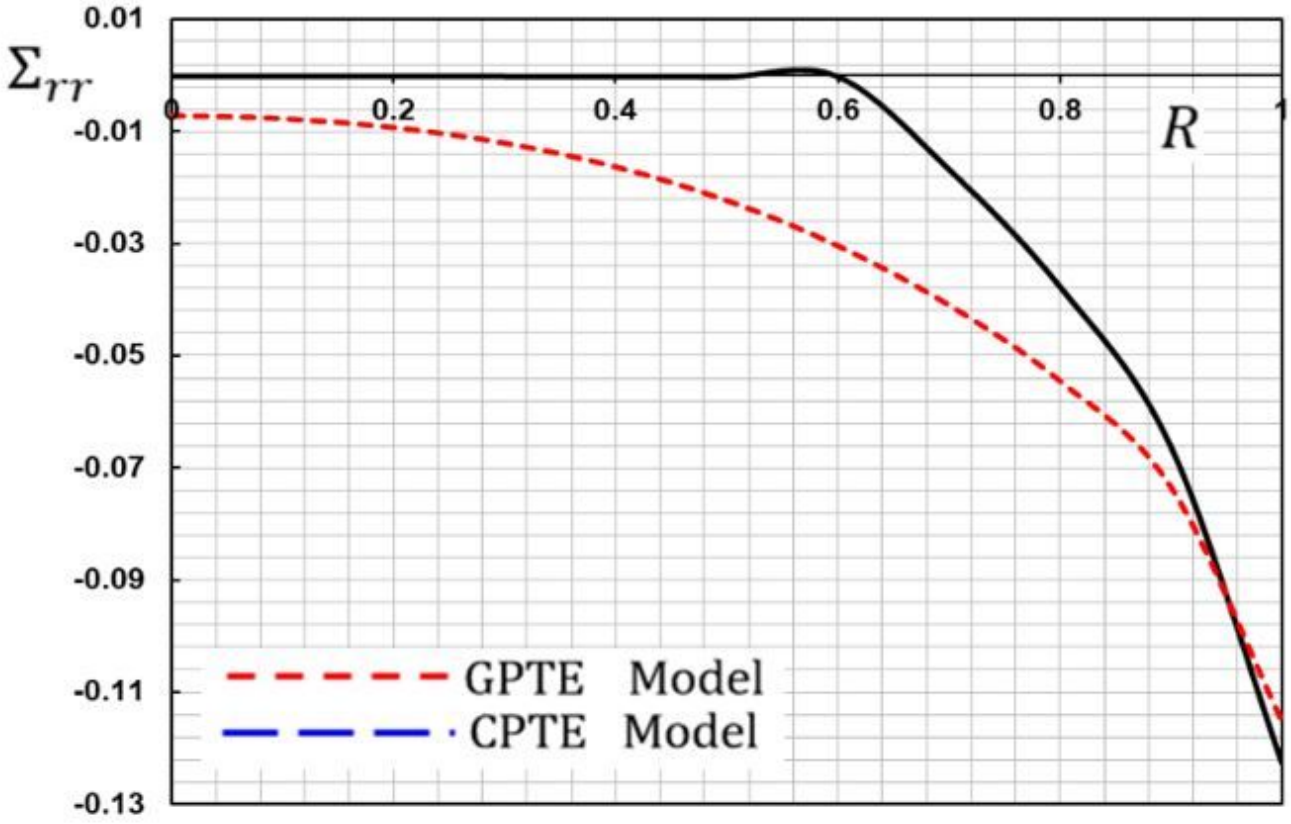

Figure 9

Variation of the stress Σ_rr with radius R for different models of photo-thermoelasticity.

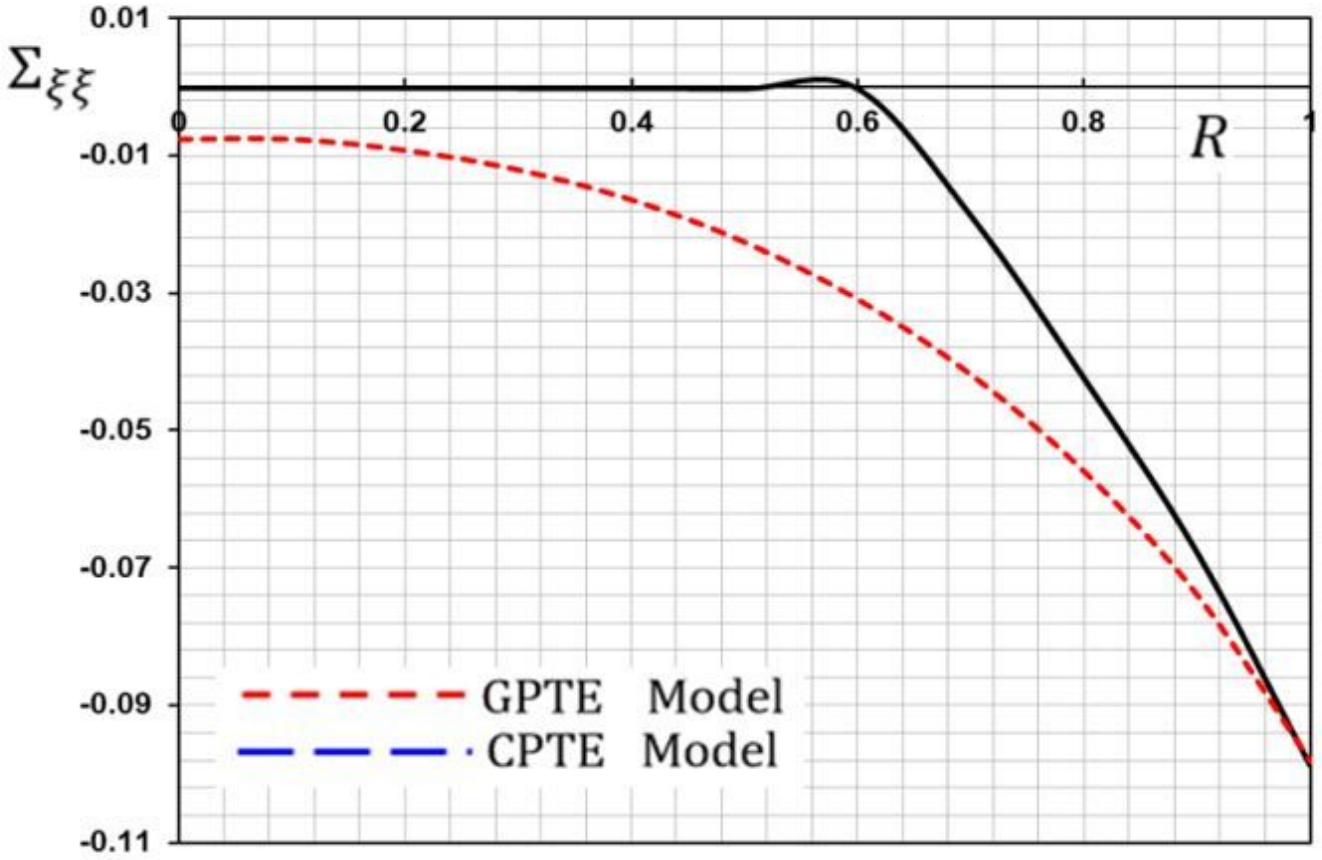

Figure 10

Variation of the stress Σ_ξξ with radius R for different models of photo-thermoelasticity.

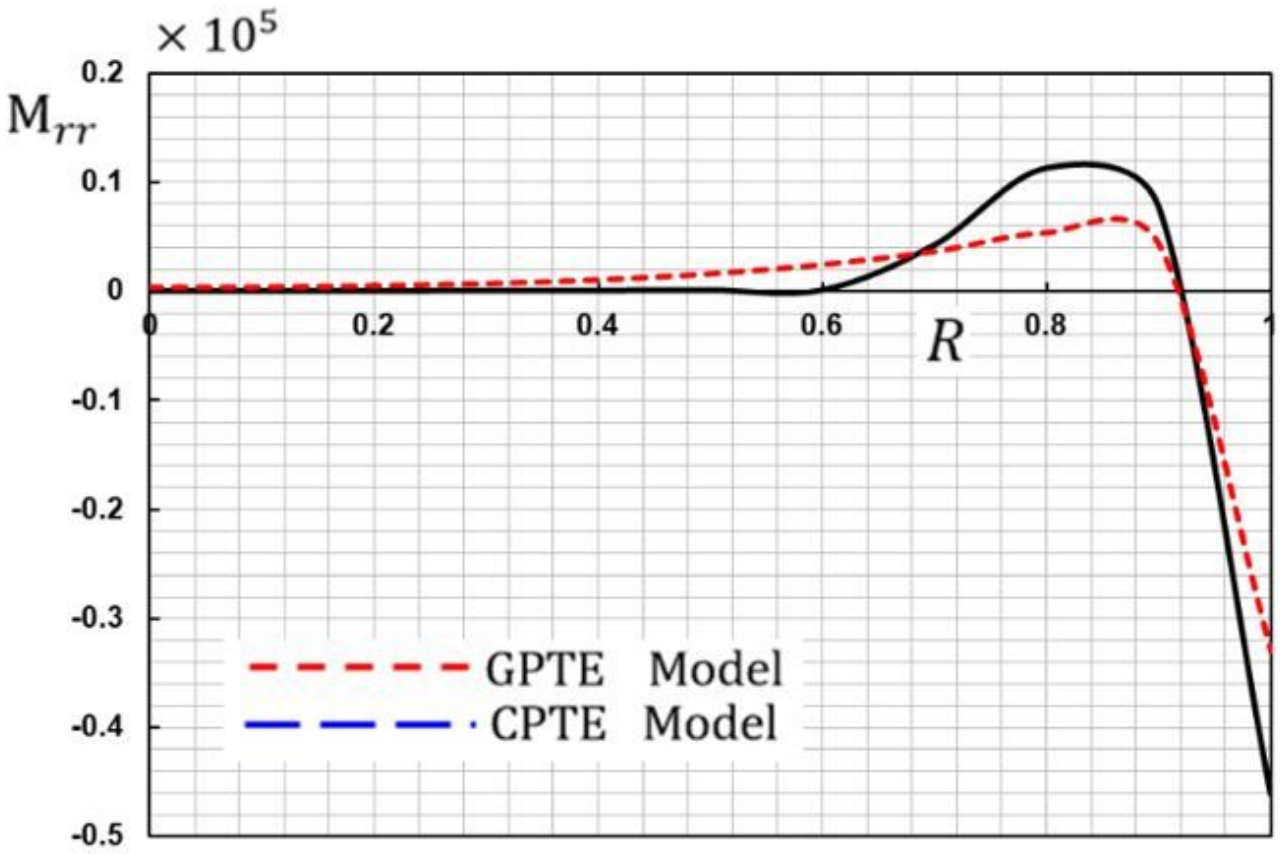

Figure 11

Variation of Maxwell's stress M_rr with radius R for different models of photo-thermoelasticity.

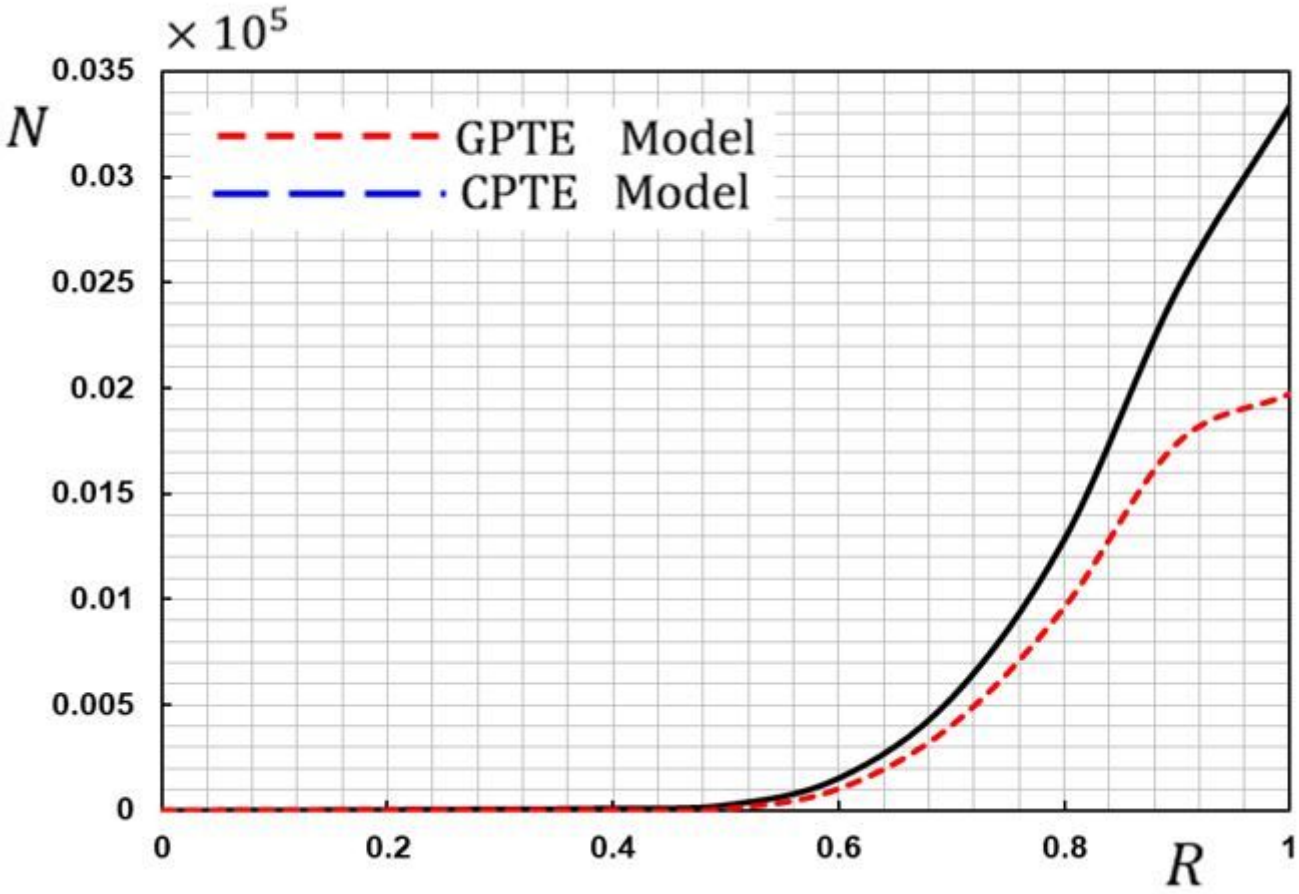

Figure 12

Variation of carrier density N with radius R for different models of photo-thermoelasticity.

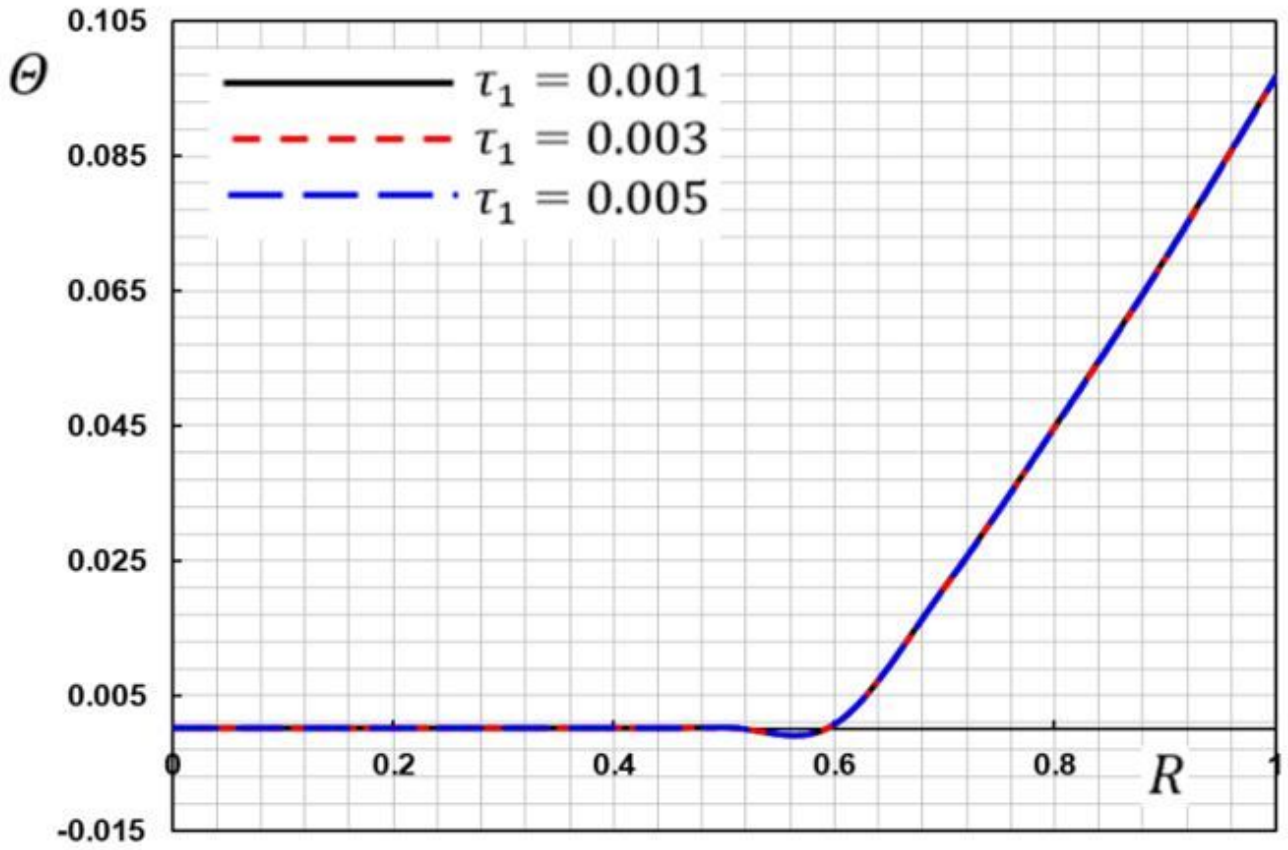

Figure 13

Variation of temperature Θ with radius R for different models of photo-thermoelasticity.

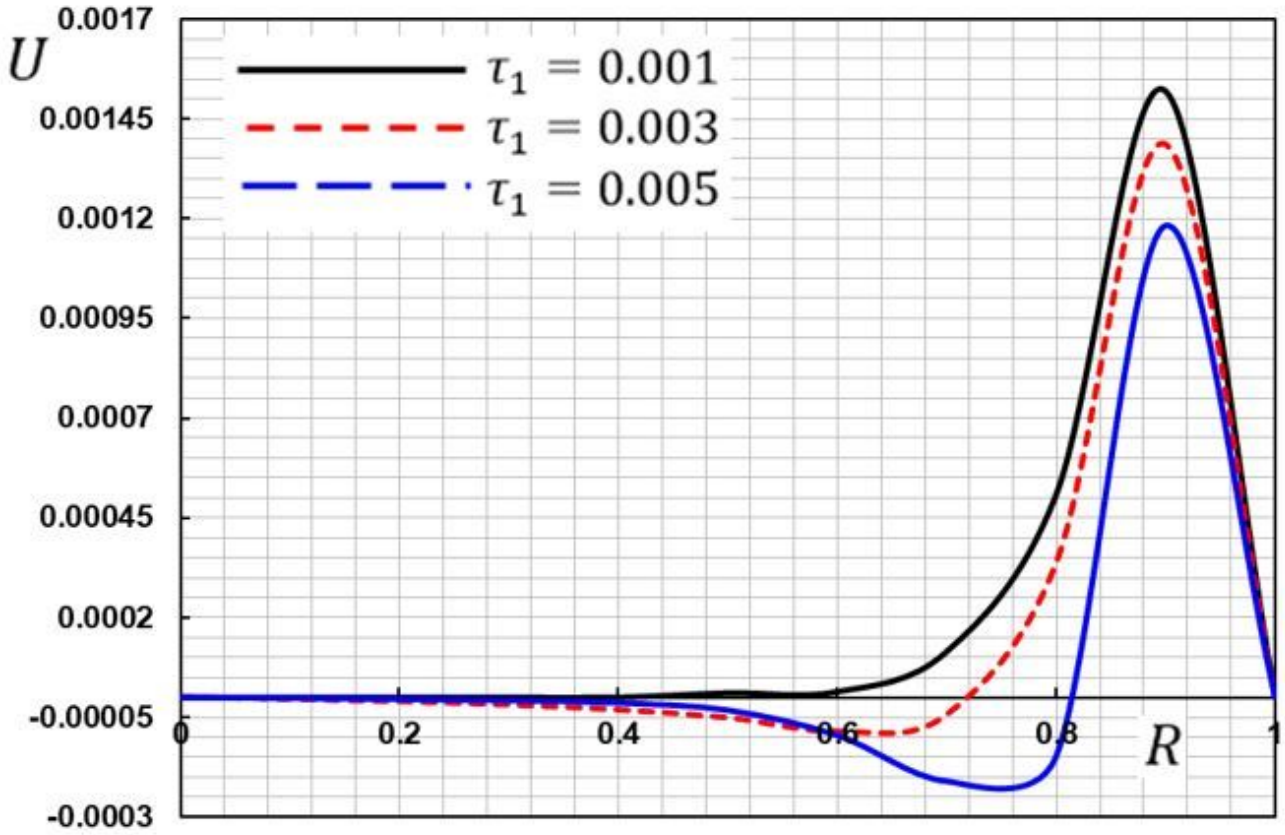

Figure 14

Variation of displacement U with radius R for different models of photo-thermoelasticity.

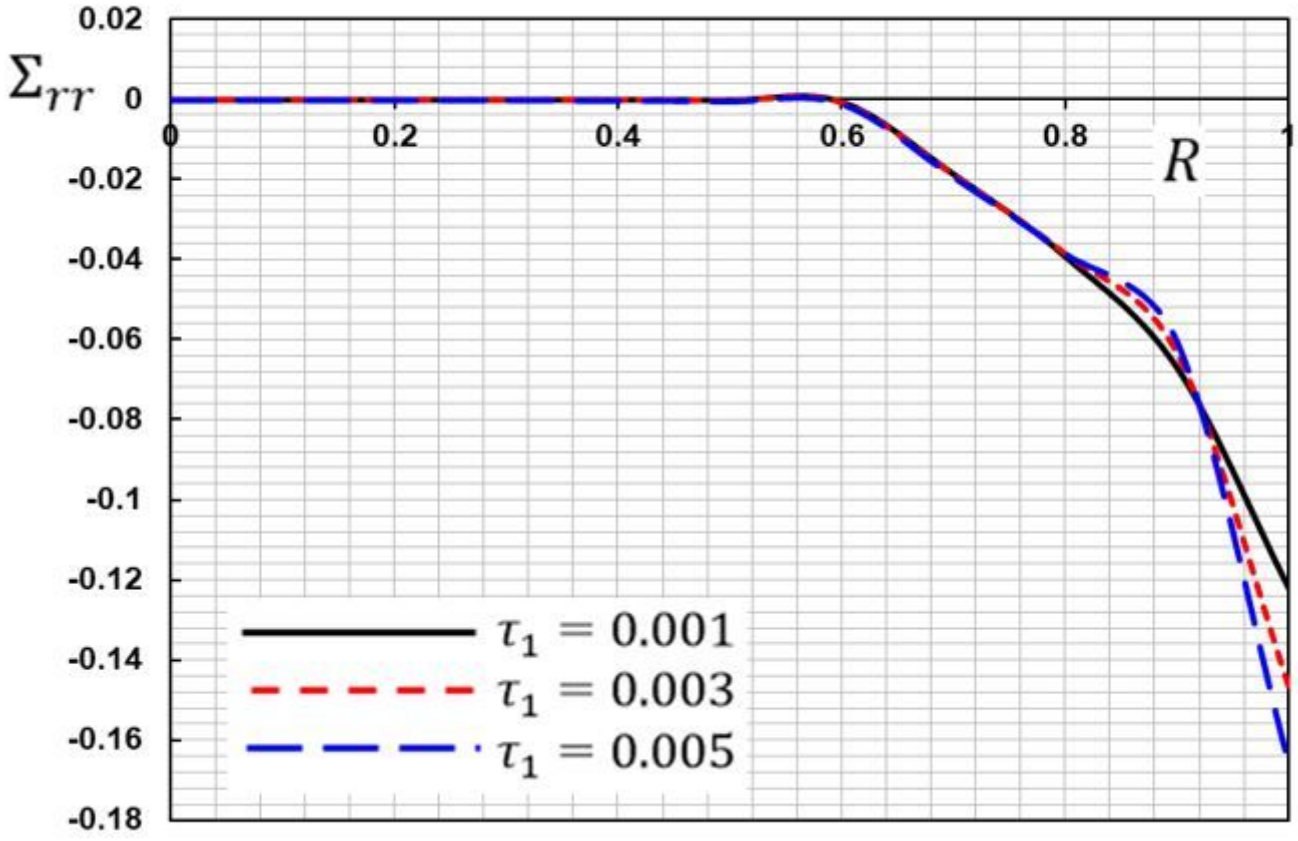

Figure 15

Variation of the stress Σ_rr with radius R for different models of photo-thermoelasticity.

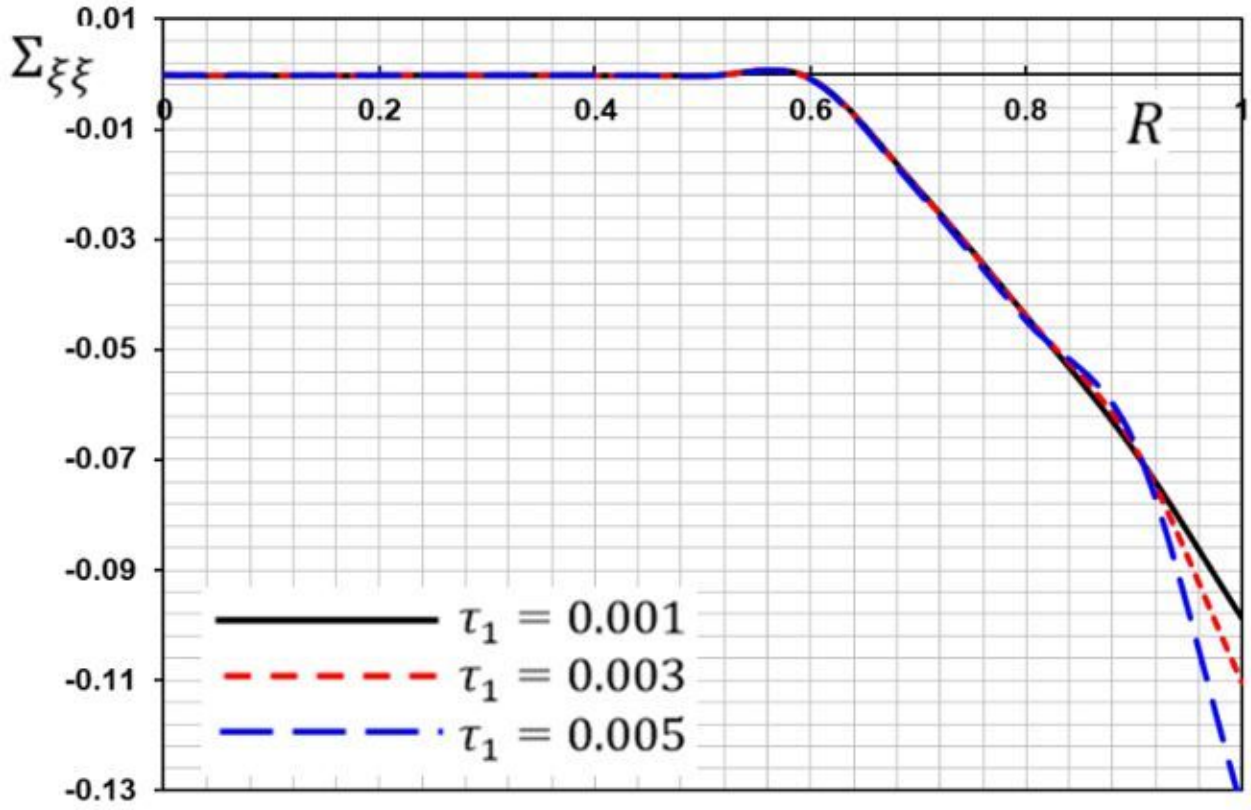

Figure 16

Variation of the stress Σ_ξξ with radius R for different models of photo-thermoelasticity.

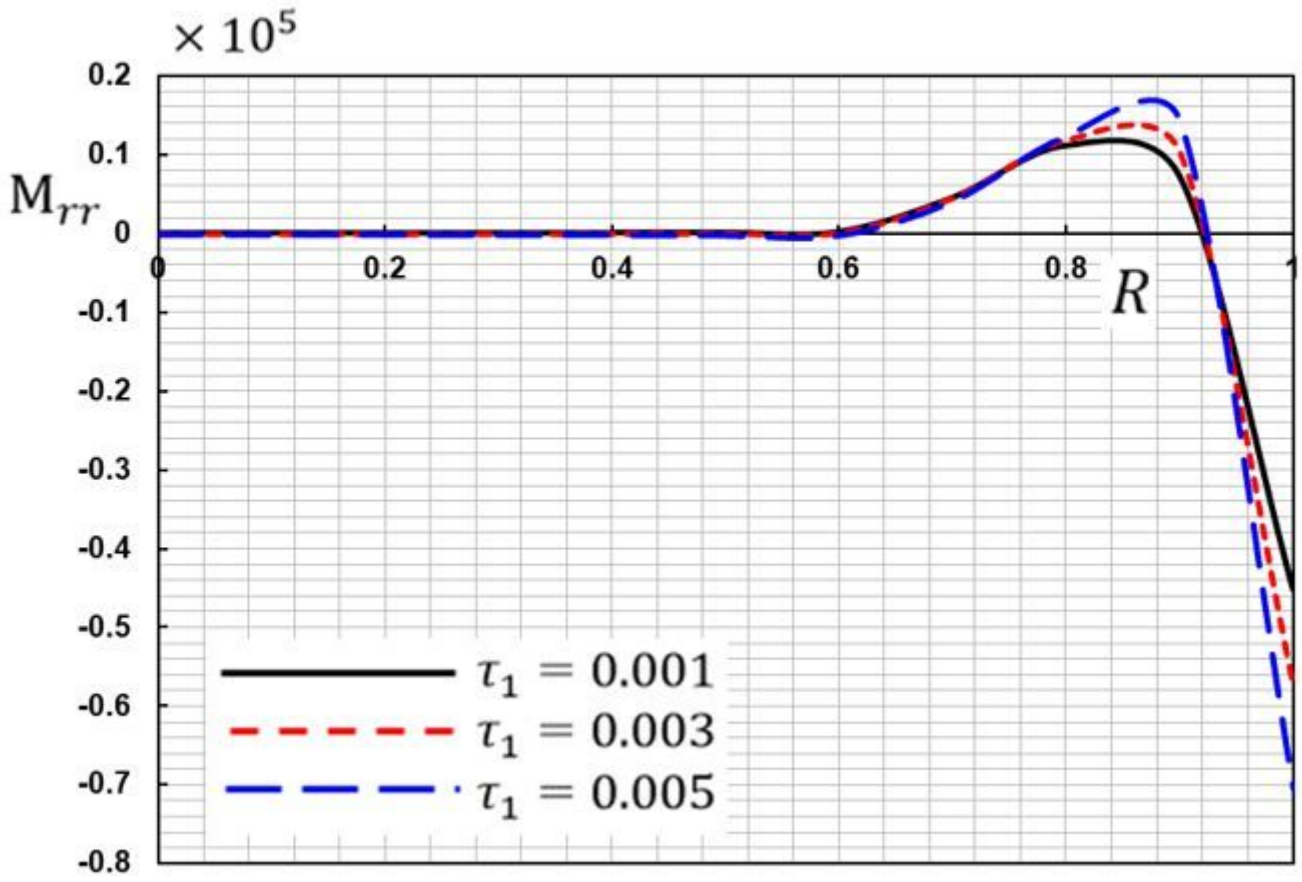

Figure 17

Variation of Maxwell's stress M_rr with radius R for different models of photo-thermoelasticity.

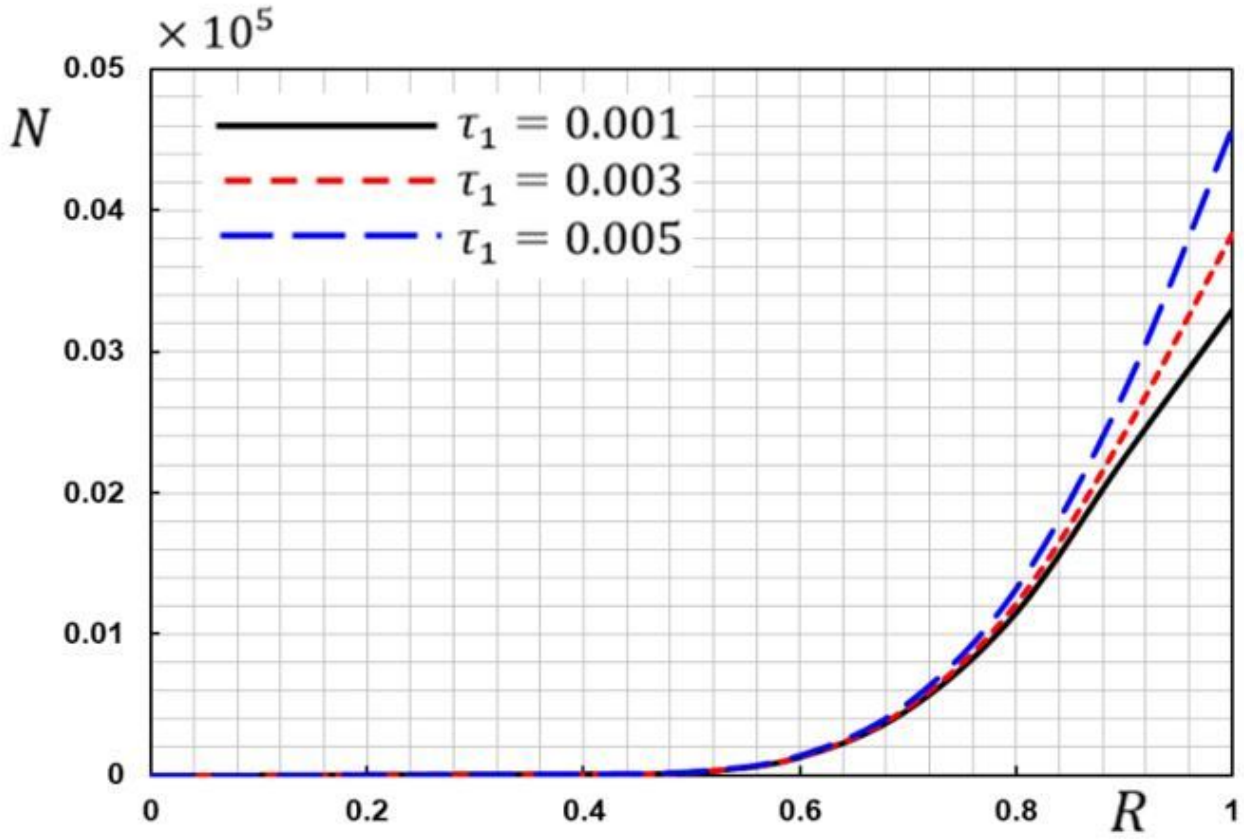

Figure 18

Variation of carrier density N with radius R for different models of photo-thermoelasticity.

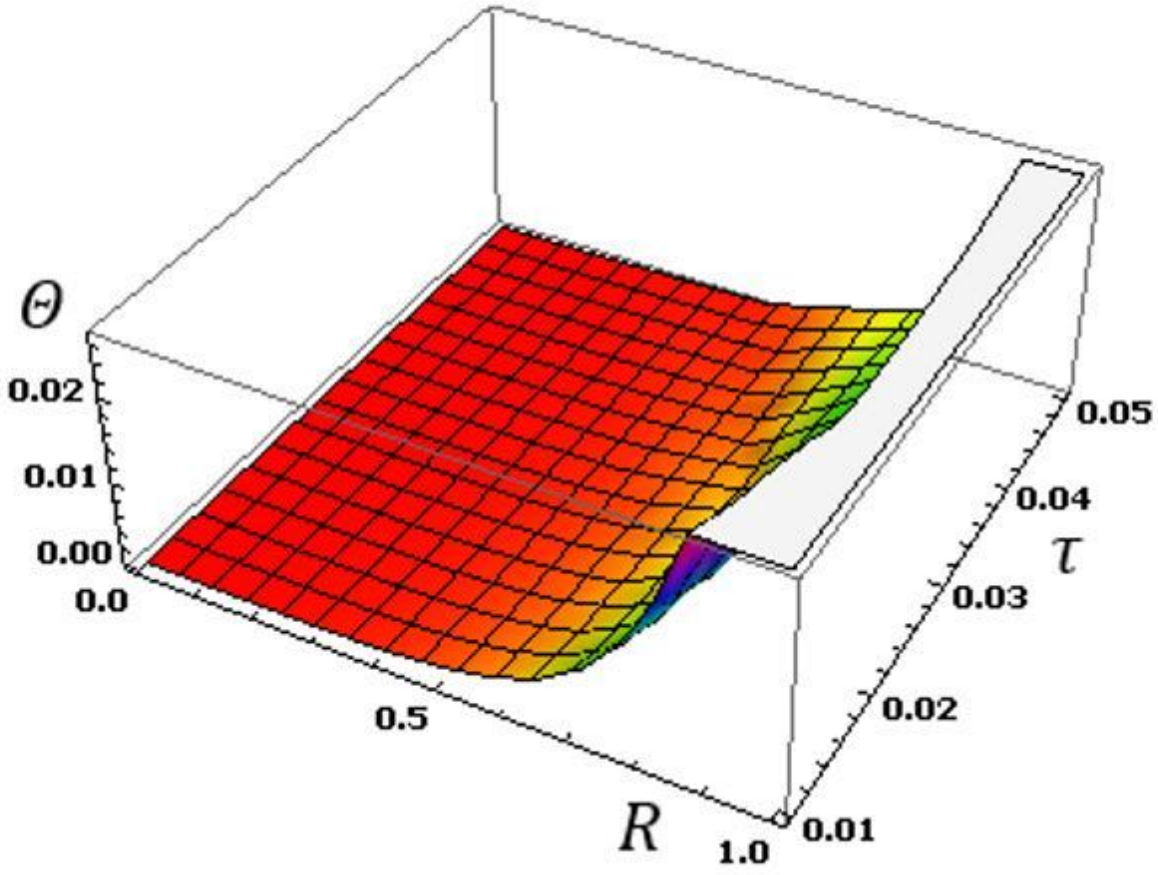

Figure 19

Variation of the temperature Θ with radius R and time τ.

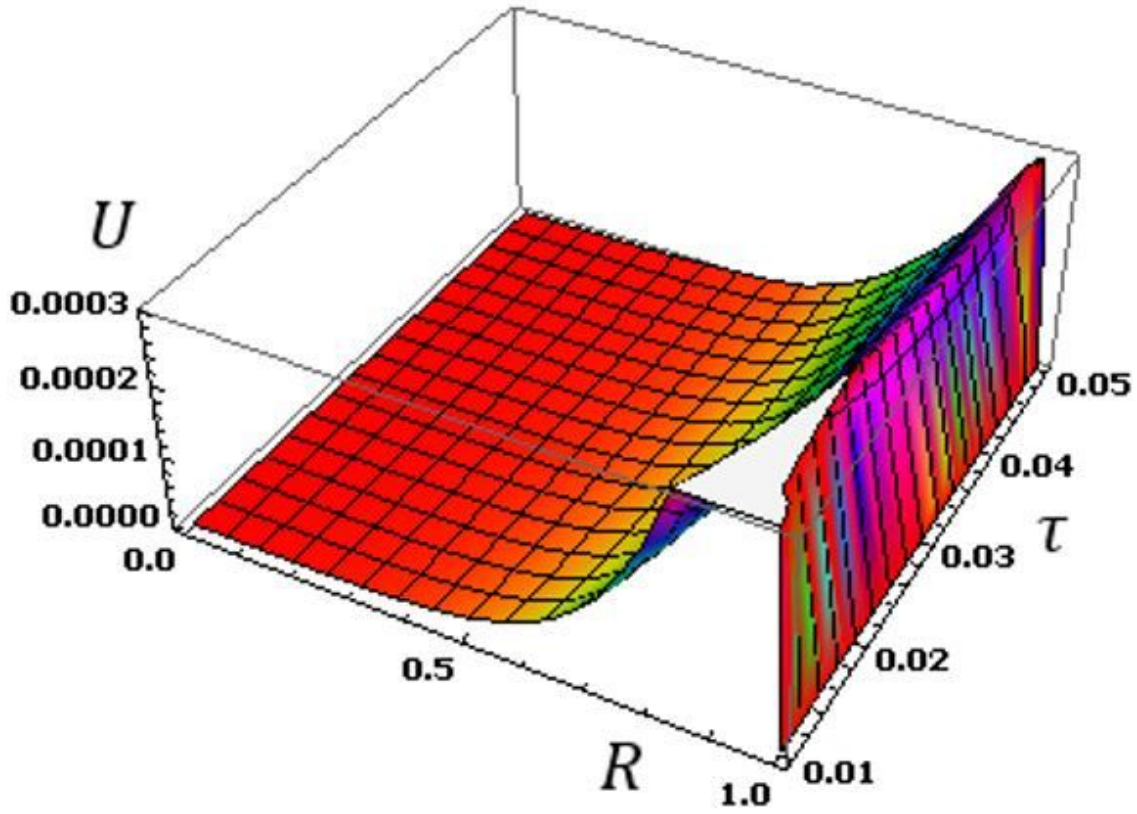

Figure 20

Variation of the displacement U with radius R and time τ.

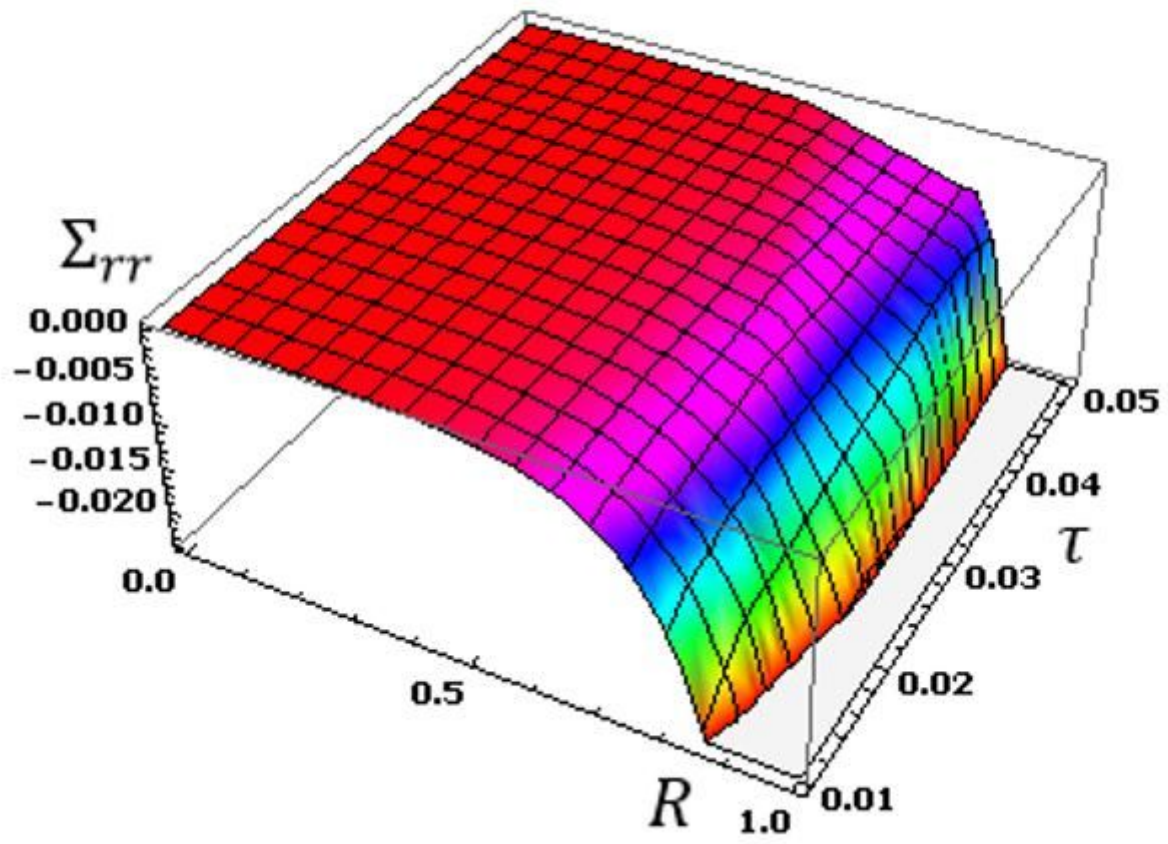

Figure 21

Variation of the stress Σ_rr with radius R and time τ.

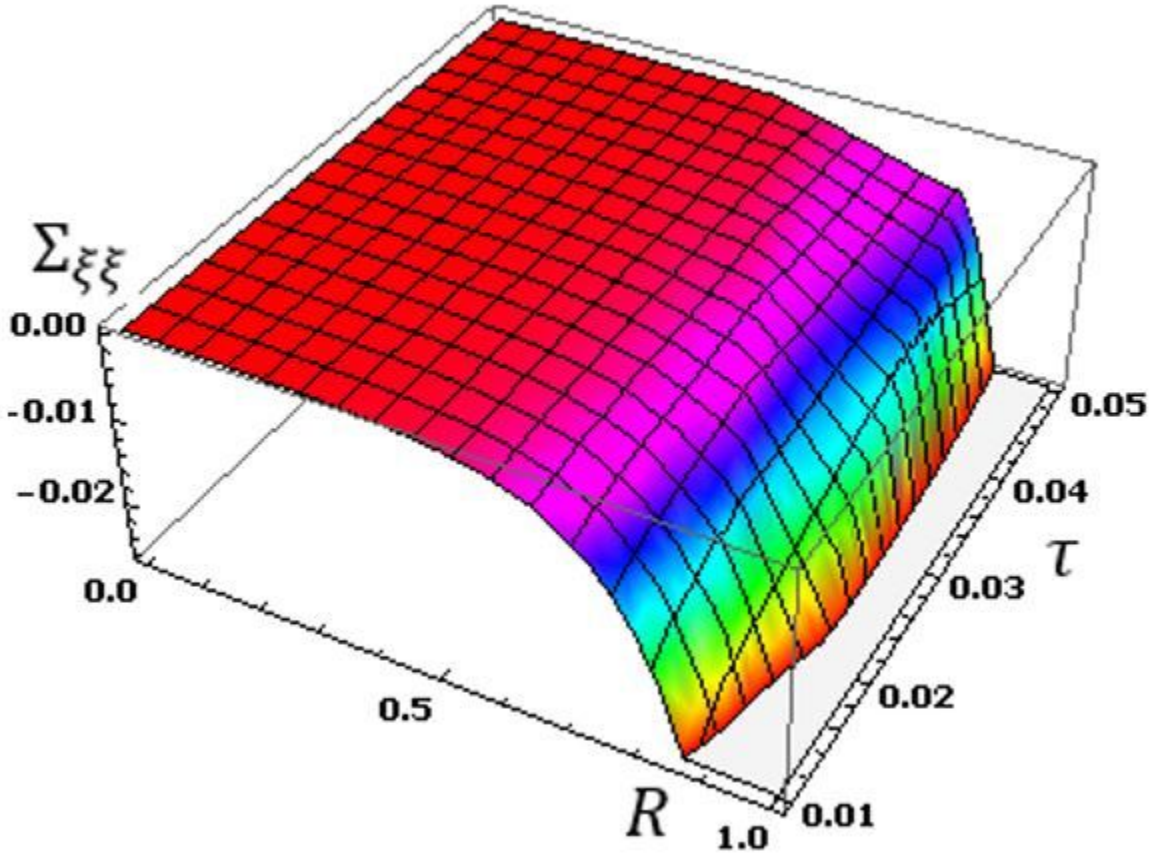

Figure 22

Variation of the stress Σ_ξξ with radius R and time τ.

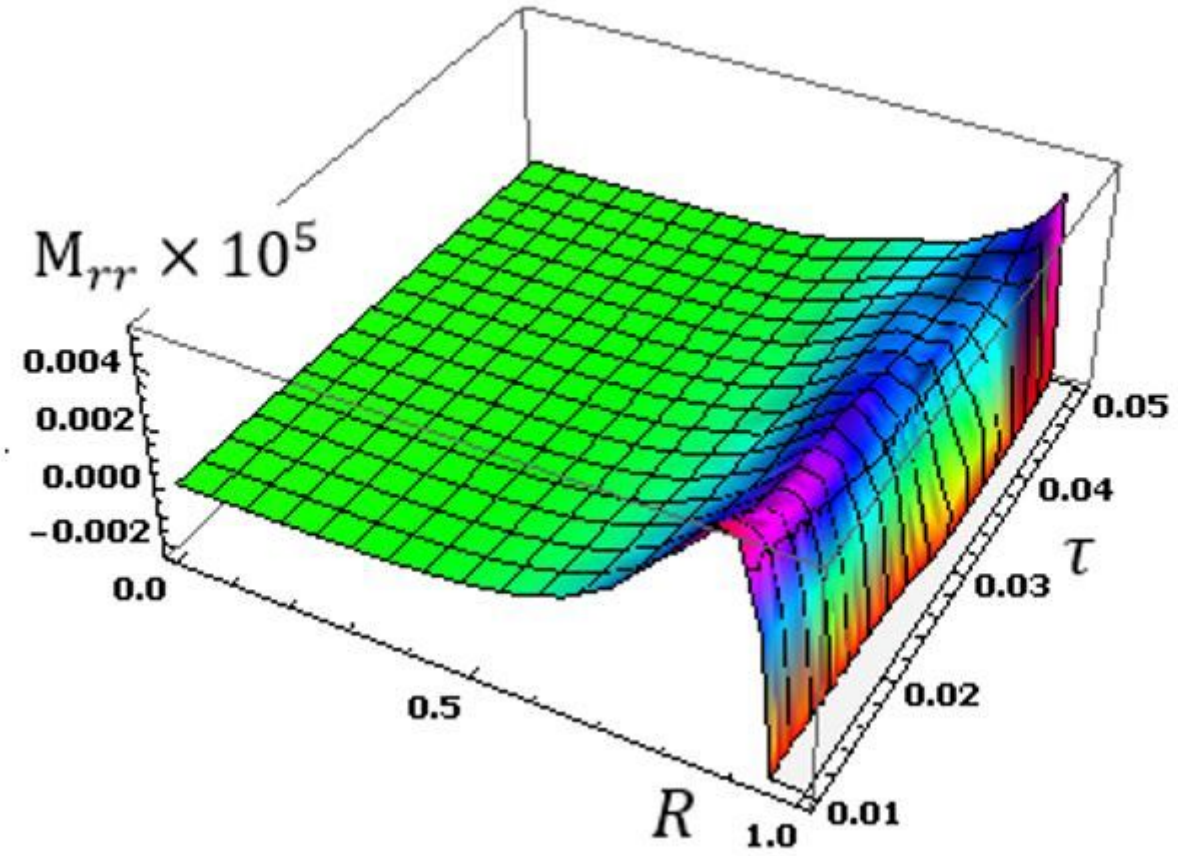

Figure 23

Variation of Maxwell's stress M_rr with radius R and time τ.

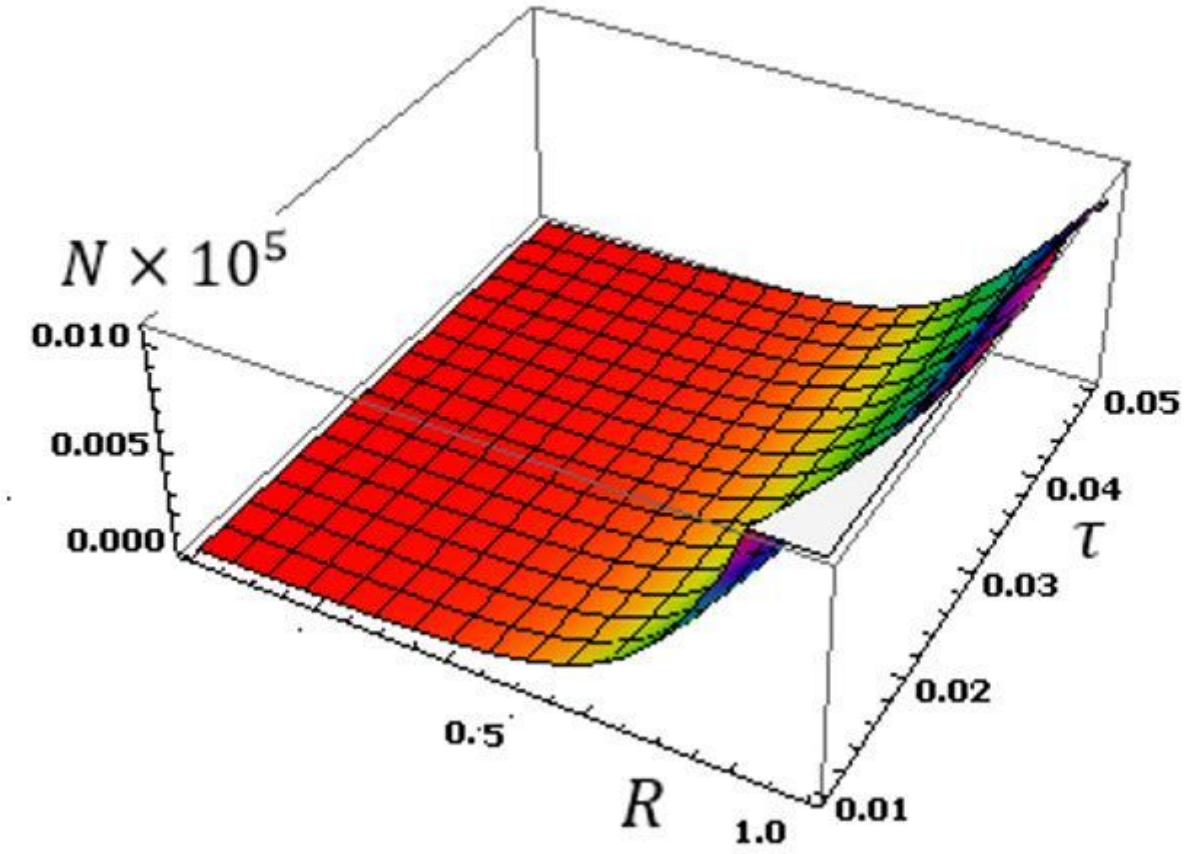

Figure 24

Variation of carrier density N with radius R and time τ.